© 2016. Published by The Company of Biologists Ltd | Journal of Cell Science (2016) 129, 2285 doi:10.1242/jcs.191569

CORRECTION

The endocytic activity of the flagellar pocket in *Trypanosoma brucei* is regulated by an adjacent phosphatidylinositol phosphate kinase

Lars Demmel, Katy Schmidt, Louise Lucast, Katharina Havlicek, Armin Zankel, Tina Koestler, Viktoria Reithofer, Pietro de Camilli and Graham Warren

There was an error published in *J. Cell Sci.* **127**, 2351–2364.

The gene ID of TbPIPKA (Tb427.04.1620) in *Trypanosoma brucei* strain 927 is Tb927.4.1620, and not Tb927.10.1620 as stated in the text.

The authors apologise to the readers for any confusion that this error might have caused.

© 2014. Published by The Company of Biologists Ltd | Journal of Cell Science (2014) 127, 2351–2364 doi:10.1242/jcs.146894

RESEARCH ARTICLE

The endocytic activity of the flagellar pocket in *Trypanosoma brucei* is regulated by an adjacent phosphatidylinositol phosphate kinase

Lars Demmel[1,*], Katy Schmidt[2,*], Louise Lucast[3], Katharina Havlicek[1], Armin Zankel[4], Tina Koestler[5], Viktoria Reithofer[6], Pietro de Camilli[3] and Graham Warren[1,‡]

ABSTRACT

Phosphoinositides are spatially restricted membrane signaling molecules. Phosphatidylinositol 4,5-bisphosphate [PI(4,5)P_2] – a phosphoinositide that is highly enriched in, and present throughout, the plasma membrane – has been implicated in endocytosis. *Trypanosoma brucei* has one of the highest known rates of endocytosis, a process it uses to evade the immune system. To determine whether phosphoinositides play a role in endocytosis in this organism, we have identified and characterized one of the enzymes that is responsible for generating PI(4,5)P_2. Surprisingly, this phosphoinositide was found to be highly concentrated in the flagellar pocket, the only site of endocytosis and exocytosis in this organism. The enzyme (designated TbPIPKA, annotated as Tb927.10.1620) was present at the neck of the pocket, towards the anterior-end of the parasite. Depletion of TbPIPKA led to depletion of PI(4,5)P_2 and enlargement of the pocket, the result of impaired endocytosis. Taken together, these data suggest that TbPIPKA and its product PI(4,5)P_2 are important for endocytosis and, consequently, for homeostasis of the flagellar pocket.

KEY WORDS: *Trypanosoma brucei*, PIP kinase, PI(4,5)P_2, Endocytosis, Flagellar pocket

INTRODUCTION

The protist parasite *Trypanosoma brucei* is the causative agent of African trypanosomiasis in man (also known as sleeping sickness) and nagana in cattle. *T. brucei* cycles between the tsetse fly (its insect vector) and its intermediate mammalian host. The main lifecycle stages used in the laboratory are the procyclic form (PCF), typically found in the fly mid-gut, and the bloodstream form (BSF) that lives in the mammalian blood or lymphatic system (Matthews, 2005).

[1]Max F. Perutz Laboratories, University of Vienna, Medical University of Vienna, 1030 Vienna, Austria. [2]Department of Cell Biology and Ultrastructure Research, Center for Anatomy and Cell Biology, Medical University of Vienna, 1090 Vienna, Austria. [3]Department of Cell Biology, Howard Hughes Medical Institute, and Program in Cellular Neuroscience, Neurodegeneration and Repair, Yale University School of Medicine, New Haven, CT 06510, USA. [4]Institute for Electron Microscopy, Graz University of Technology and Center for Electron Microscopy Graz, 8010 Graz, Austria. [5]Center for Integrative Bioinformatics, Max F. Perutz Laboratories, University of Vienna and Medical University of Vienna, 1030 Vienna, Austria. [6]University of Applied Sciences Wiener Neustadt, Department of Biomedical Analytics, 2700 Wiener Neustadt, Austria.
*These authors contributed equally to this work

‡Author for correspondence (Graham.Warren@mfpl.ac.at)

Received 22 November 2013; Accepted 15 February 2014

As an extracellular parasite, *T. brucei* is constantly exposed to the host immune system and has, therefore, developed multiple ways to evade the immune response. One means of immune evasion is the continuous and very rapid uptake of surface-bound antibodies. Antibodies that have attached to the variable surface glycoprotein (VSG) are rapidly and selectively swept towards the flagellar pocket, a small invagination of the plasma membrane near the posterior of the cell, where the flagellum exits the cell. This sweeping towards the flagellar pocket is thought to occur by the hydrodynamic flow of the extracellular medium over the cell surface as the cell moves forward by the beating of the flagellum. Selectivity is imparted by the fact that the antibodies that are bound to the VSG act as molecular 'sails', which result in very rapid and preferential movement of the antibody–VSG complex towards the flagellar pocket. After endocytosis and processing in the endosomes, the VSG is recycled back to the plasma membrane, whereas the antibodies are delivered to the lysosome and degraded (Engstler et al., 2007; Engstler et al., 2004). Thus, endocytosis is essential to this parasite, not only for nutrient uptake but also for survival in a hostile environment. In fact, BSF cells have one of the highest rates of endocytosis of any known eukaryote (Engstler et al., 2004). Endo- and exocytosis take place exclusively in the flagellar pocket in *T. brucei* (Allen et al., 2003; Engstler et al., 2004; Overath and Engstler, 2004).

Endocytosis is strictly clathrin-dependent in both procyclic and bloodstream *T. brucei* (Allen et al., 2003; Hung et al., 2004). Clathrin-mediated endocytosis has been observed in all complex eukaryotes, where it plays a role in a wide variety of cellular functions, such as nutrient uptake, regulation of protein abundance at the cell surface, cellular signaling and the uptake of surface components destined for degradation or recycling. Clathrin-mediated endocytosis is a multistep process comprising nucleation, cargo selection, coat assembly, scission and uncoating (McMahon and Boucrot, 2011). At least in mammalian cells, all these steps are crucially dependent on phosphatidylinositol 4,5-bisphosphate [PI(4,5)P_2], a phosphoinositide that is concentrated in the plasma membrane, and all endocytic clathrin adaptors, and most of the other membrane-associated factors that participate in this process, bind to this phosphoinositide (McLaughlin and Murray, 2005; Di Paolo and De Camilli, 2006). For example, PI(4,5)P_2 recruits the clathrin-coat nucleation factors, such as the FCH-domain-only (FCHO) proteins 1 and 2, to the cytoplasmic leaflet of the plasma membrane (Henne et al., 2010; Mulkearns and Cooper, 2012; Stimpson et al., 2009). PI(4,5)P_2 also localizes the adaptor protein 2 complex (AP2), which is involved in cargo selection, to clathrin-coated pits (Collins et al., 2002; Gaidarov and Keen, 1999; Kelly et al., 2008). PI(4,5)P_2 also interacts with

Journal of Cell Science (2014) 127, 2351–2364 doi:10.1242/jcs.146894

AP2 accessory proteins – such as those containing the AP180 N-terminal homology (ANTH) domain or the epsin N-terminal homology (ENTH) domain, which have roles in membrane binding and membrane bending, respectively (Ford et al., 2002; Ford et al., 2001). After cargo capture, AP2, together with several accessory proteins, recruits clathrin to the membrane and clathrin-coated vesicles are formed (Dell'Angelica et al., 1998; Edeling et al., 2006a; Edeling et al., 2006b; ter Haar et al., 2000; Knuehl et al., 2006). To complete scission of the budding vesicles, dynamin must be recruited to the neck of clathrin-coated pits, and this recruitment requires the interaction of its pleckstrin homology (PH) domain with PI(4,5)P_2 (Achiriloaie et al., 1999; Hinshaw and Schmid, 1995; Kosaka and Ikeda, 1983; Sweitzer and Hinshaw, 1998). Eventually, after fission of the endocytic pit, dephosphorylation of PI(4,5)P_2 by inositol 5-phosphatases is required for coat shedding (Cremona et al., 1999; Milosevic et al., 2011). Acute depletion of PI(4,5)P_2 in mammalian cells results in a complete arrest of clathrin-mediated endocytosis, highlighting the physiological importance of these interactions (Zoncu et al., 2007). The generation of PI(4,5)P_2 is, therefore, a key step that is required for clathrin-mediated endocytosis.

The majority of PI(4,5)P_2 in mammalian cells is synthesized by phosphorylation of phosphatidylinositol 4-phosphate (PI4P) at the 5 position of the inositol ring by one of three isoforms of type I phosphatidylinositol phosphate (PIP) kinases: α, β or γ (Ishihara et al., 1996; Ishihara et al., 1998; Loijens and Anderson, 1996), and these kinases have been implicated in the generation of the pools of PI(4,5)P_2 that are responsible for clathrin-mediated endocytosis (Krauss et al., 2003; Krauss et al., 2006; Thieman et al., 2009; Wenk et al., 2001). Alternatively, PI(4,5)P_2 can also be generated by phosphorylation of phosphatidylinositol 5-phosphate (PI5P) at the 4 position by type II PIP kinases (Fruman et al., 1998; Carricaburu et al., 2003; Doughman et al., 2003).

Given the essential role of endocytosis in *T. brucei*, we investigated the degree of conservation of the machinery that is required for clathrin-coated vesicle formation. AP2 has not been identified in the *T. brucei* genome, and dynamin, though present, does not appear to be involved in endocytosis (Berriman et al., 2005; Chanez et al., 2006; Morgan et al., 2004). However, one ENTH domain protein that might bind to PI(4,5)P_2 is present in *T. brucei* (TbEpsinR; Gabernet-Castello et al., 2009). We, therefore, investigated the generation of PI(4,5)P_2 in *T. brucei* and asked whether, and to what extent, it is involved in endocytosis. Here, we identify a novel protein with PIP kinase activity in *T. brucei* (TbPIPKA); we show that it only localizes to the neck of the flagellar pocket and that its product PI(4,5)P_2 is only present in the flagellar pocket membrane and not in the contiguous outer plasma membrane. Depletion of TbPIPKA leads to a reduction of PI(4,5)P_2 levels and enlargement of the flagellar pocket with consequent inhibition of endocytosis. We, therefore, not only demonstrate a requirement for PI(4,5)P_2 in endocytosis in *T. brucei* but also in the homeostasis of the flagellar pocket.

RESULTS

The T. brucei genome encodes three putative PI4P 5-kinase orthologues

Tb427.04.1620, Tb427.10.3890 and Tb427.10.4770 are annotated in the *T. brucei* genome as PIP kinases (Aslett et al., 2010). To explore the degree of conservation of primary structure of these three *T. brucei* proteins, a multiple sequence alignment was performed. Their predicted catalytic lipid kinase domains were aligned against the catalytic domains of *Saccharomyces cerevisiae* ScMss4p (a PI4P 5-kinase) and human HsPIPKIα and HsPIPKIIα (Fig. 1). The alignment shows strong sequence conservation (gray background) for all three putative PIP kinases. Importantly, many residues that are implicated in ATP-binding (red background), as well as in catalytic activity (green background), are conserved. Tb427.04.1620 shares an amino acid sequence identity of 37%, 43% and 38% with ScMss4p, HsPIPIα and HsPIPKIIα, respectively. The corresponding amino acid sequence similarities are 53%, 46% and 45%. In this paper, we have focused on Tb427.04.1620 because this yielded the most interesting pattern of localization and refer to it throughout as TbPIPKA (see Discussion).

TbPIPKA has PIP kinase activity

To test whether TbPIPKA has PI4P 5-kinase activity, a stable procyclic cell line that expressed a Ty1-tagged TbPIPKA fusion protein under an inducible promoter was generated. Cells were grown for 15 h in the absence or presence of 7.5 ng/ml or 100 ng/ml doxycycline. Immunoblots of *T. brucei* cell lysates using antibodies against Ty1 confirmed the increased expression of Ty1–TbPIPKA (Fig. 2A). We next determined whether exogenous expression of Ty1–TbPIPKA increased the production of PI(4,5)P_2. Anionic lipids were extracted and subjected to a conductivity-detection-based high-pressure liquid chromatography (HPLC) analysis, which allows separation of mono- and di-phosphorylated phosphatidylinositol (PIP and PIP_2, respectively) (Nasuhoglu et al., 2002). The amounts of PIP_2 and PIP, are expected to reflect primarily PI(4,5)P_2 and PI4P, respectively, because these two phophoinositides typically represent the most abundant PIP_2 and PIP species (Di Paolo and De Camilli, 2006). These were measured and their ratio determined (Fig. 2B). In the absence of doxycycline, the basal value of PIP_2:PIP was 0.36, representing, presumably, the activity of endogenous PIP kinases. Induction of Ty1–TbPIPKA with 7.5 ng/ml doxycycline increased the PIP_2:PIP ratio to 0.55, whereas 100 ng/ml doxycycline increased the ratio to 2.2 (Fig. 2B). Superimposition of the HPLC profiles of the control samples with those of samples that had been induced with 100 ng/ml doxycycline showed that the increase in the PIP_2:PIP ratio was owing to raised PIP_2 [PI(4,5)P_2)] levels at the expense of the PIP precursor (PI4P) (Fig. 2C).

Knockdown of TbPIPKA in PCF and BSF cells

In order to study the effects of TbPIPKA depletion, cell lines in which RNA interference (RNAi) against TbPIPKA could be induced were generated using both PCF and BSF cells. The expression of TbPIPKA was silenced by the induction of double-stranded RNA upon the addition of doxycycline.

For both cell lines, growth slowed after a day and stopped after 5 days (Fig. 3A). To measure the effect of TbPIPKA depletion on the cell cycle, the number of kinetoplasts (mitochondrial DNA) and nuclei were counted. At the start of the cell cycle, which generally takes about 9 h to complete in the PCF and BSF, cells have one nucleus and one kinetoplast. The kinetoplast duplicates first and segregates, resulting in cells harboring one nucleus and two kinetoplasts. The nucleus divides later giving rise to cells with two nuclei and two kinetoplasts. Cytokinesis then generates two daughter cells that, again, have one nucleus and one kinetoplast. If, however, the cell cycle is affected, abnormal DNA states, such as two nuclei and one kinetoplast, one nucleus and no kinetoplasts or zoids (no nucleus and one kinetoplast), can occur.

Journal of Cell Science (2014) 127, 2351–2364 doi:10.1242/jcs.146894

Fig. 1. Multiple sequence alignment of PIP kinase domains. The sequences of ScMss4p, HsPIPKIα and HsPIPKIIα were aligned with the sequences of the *T. brucei* proteins Tb427.04.1620, Tb427.10.4770 and Tb427.10.3890 using MAFFT software. Only the PI4P 5-kinase Pfam domain is shown here. Conserved residues are highlighted with a gray background. Residues implicated in ATP-binding are indicated with a red background, amino acids thought to be in the catalytic core are marked in green. The region within the activation loop, which determines substrate specificity, is marked with a red box and suggests that Tb427.04.1620 is more closely related to type I, rather than type II, PIP kinases. Tb427.04.1620 is designated TbPIPKA throughout the manuscript.

TbPIPKA RNAi cells were induced for up to 3 days and samples were taken after 2 or 3 days from control and TbPIPKA-depleted cells. No changes in the cell-cycle stages were observed. Moreover, none of the abnormal cell-cycle stages accumulated in TbPIPKA-depleted cells (Fig. 3B). These data suggest a homeostatic effect of TbPIPKA depletion on cell growth.

To determine the efficiency of TbPIPKA knockdown, RNA was prepared from control and TbPIPKA-depleted cells after 3 days. Depletion of TbPIPKA in PCF and BSF cells resulted in downregulation of the TbPIPKA mRNA levels by 67% and almost 100%, respectively (Fig. 3C).

To assess the production of $PI(4,5)P_2$ after TbPIPKA depletion, lipids from control and TbPIPKA-depleted cells were extracted after 3 days and subjected to HPLC analysis. Depletion of TbPIPKA resulted in the reduced production of $PI(4,5)P_2$, as shown by the decrease in PIP_2:PIP ratio compared to that of control cells (0.26 versus 0.17) (Fig. 3D). Together with the overexpression studies, these data strongly suggest that TbPIPKA has PI4P 5-kinase activity.

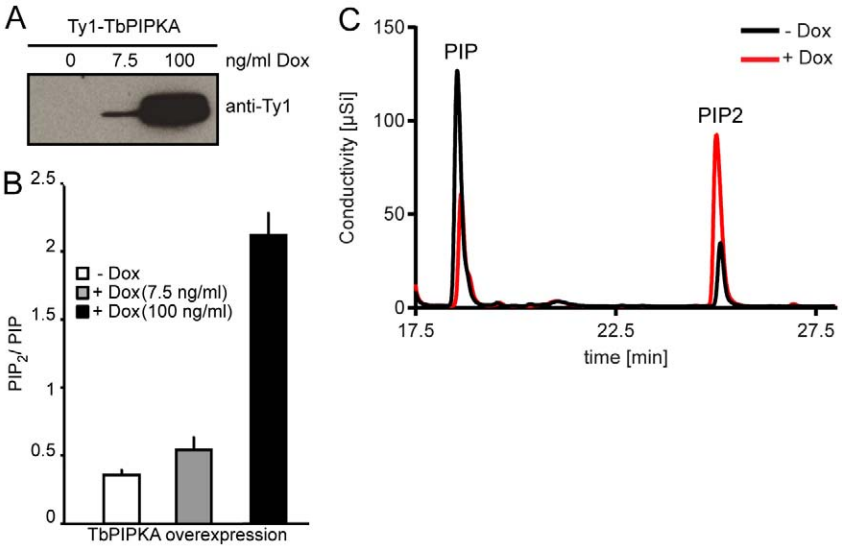

Fig. 2. Overexpression of TbPIPKA increases PIP_2 levels. PCF cells were stably transfected with pLew100-Ty1-TbPIPKA. Expression of the fusion proteins was induced using the indicated amounts of doxycycline (Dox) for 15 hours. (A) Tagged proteins from total cell lysates were detected using monoclonal antibodies against Ty1. (B) Lipids were extracted from 8×10^{10} cells and subjected to HPLC analysis. The peak area ratio of PIP_2 to PIP was calculated and an increase in the PIP_2:PIP ratio was observed following increased expression of Ty1–TbPIPKA. The basal ratio in the absence of doxycycline is likely caused by the activity of endogenous PIP kinases. Results are presented as the mean of three independent experiments±s.e.m. (C) Overlaid output traces obtained during HPLC analysis of lipids from cells that had been transfected with pLew-Ty1-TbPIPKA growing in the absence (−Dox) or presence (+Dox) of 100 ng/ml doxycycline. Note that the increase in PIP_2 is accompanied by a decrease in PIP, suggesting that Tb427.04.1620 is a PIP kinase.

Journal of Cell Science (2014) 127, 2351–2364 doi:10.1242/jcs.146894

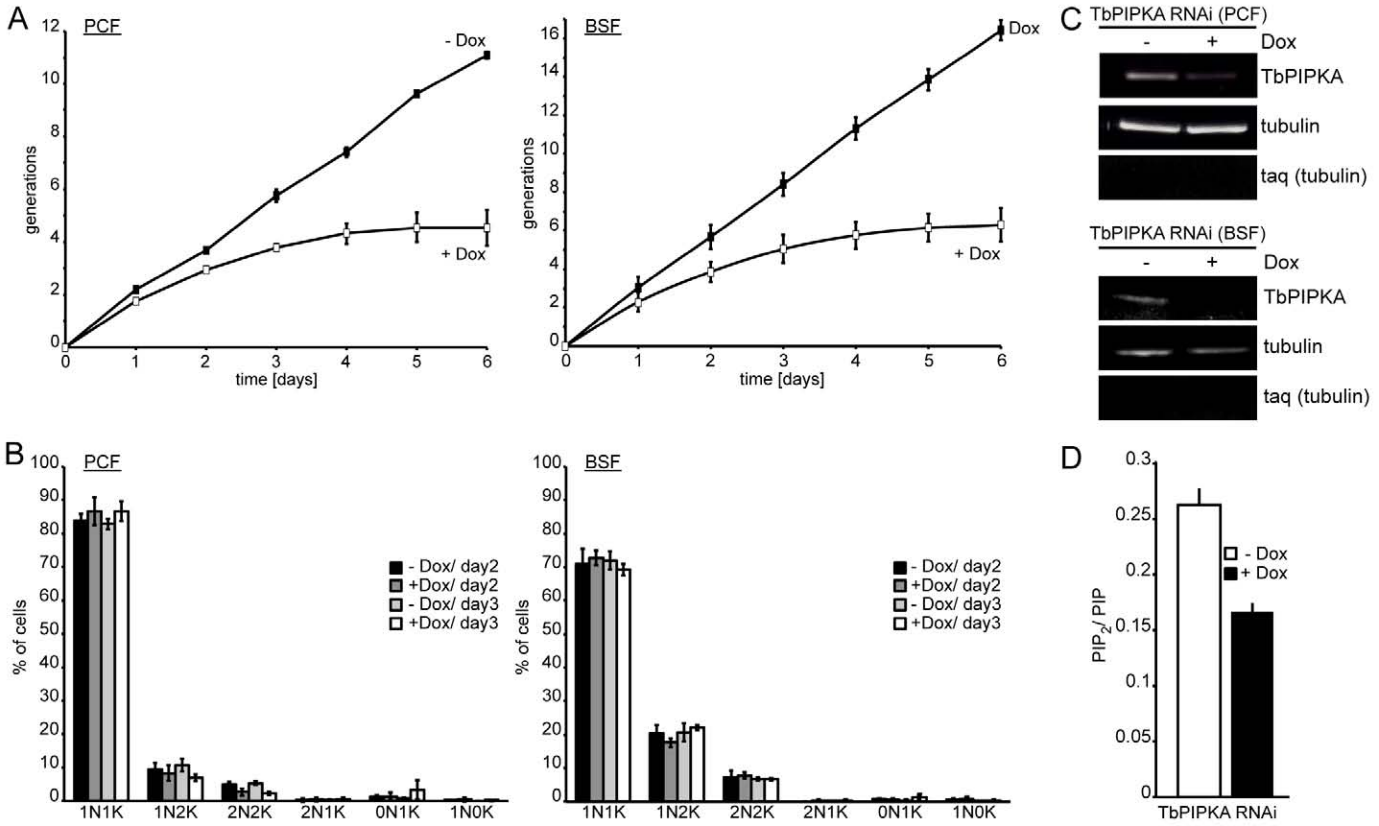

Fig. 3. Depletion of TbPIPKA by RNAi. (A) TbPIPKA depletion (+Dox) caused a growth arrest in PCF and BSF cells. Data points are the means±s.e.m., $n=3$. (B) Depletion of TbPIPKA does not cause a cell-cycle progression defect in PCF (left panel) or BSF (right panel) cells. Samples of control (−Dox) and induced-RNAi (+Dox) from PCF and BSF cells were taken after 2 and 3 days. Nuclear (N) and kinetoplast (K) DNA was labeled with DAPI to determine the cell cycle state. At least 300 cells were analyzed for each timepoint across three independent experiments. Values are mean±s.e.m., $n=3$. 1N1K, one nucleus, one kinetoplast etc. (C) TbPIPKA mRNA depletion following induction of RNAi. RNA was isolated from PCF (top panel) and BSF (bottom panel) cells after growth in the absence or presence of 100 ng/ml doxycycline for 3 days. Tubulin served as the loading control, taq (tubulin) was used to determine DNA contamination. (D) Extracted lipids from TbPIPKA-depleted (+Dox) PCF cells were analyzed by HPLC and the PIP_2:PIP peak area ratio was plotted. Three independent experiments, values are mean±s.e.m.

TbPIPKA localizes to the neck of the flagellar pocket

To characterize the subcellular localization of TbPIPKA, in both PCF and BSF cells, one allele of TbPIPKA was endogenously replaced with another that encoded TbPIPKA that was tagged with yellow fluorescent protein (YFP). The location of marker proteins is shown in Fig. 4A. The flagellum originates from the basal bodies at the base of the flagellar pocket and emerges through the neck of the flagellar pocket (Lacomble et al., 2010). The flagellar membrane is continuous with the flagellar pocket membrane and the plasma membrane of the cell (Lacomble et al., 2009). The flagellum stays attached to the cell body along the entire posterior to anterior axis through punctate transmembrane junctions, which are part of a cytoskeletal structure that is termed the flagellum attachment zone (Bastin et al., 2000). The flagellar pocket collar demarcates the flagellar pocket (Gull, 2003) and is marked by TbBILBO1, which is required for flagellar pocket biogenesis (Bonhivers et al., 2008). Between the flagellar pocket collar and the solvent-exposed plasma membrane lies the so-called flagellar pocket neck region (Henley et al., 1978). A multi-protein cytoskeletal structure termed the bilobe is located above the flagellar pocket collar (Esson et al., 2012; He et al., 2005; Morriswood et al., 2013; Morriswood et al., 2009) and is marked by TbMORN1, LRRP1 and TbCentrin4. However, their localization patterns do not overlap, indicating distinct subdomains. The TbMORN1 and LRRP1 subdomain is shaped like a fish-hook, the posterior part of which encircles the flagellar pocket neck, above the flagellar pocket collar, and partially overlaps with the posterior tip of the flagellum attachment zone. TbCentrin4 is found parallel to the anterior stem of the TbMORN1 structure (Esson et al., 2012).

YFP–TbPIPKA localized to a discrete structure between the nucleus and the kinetoplast in both lifecycle stages (Fig. 4B,C; supplementary material Fig. S1). In PCF cells, YFP–TbPIPKA was generally seen as a rod-shaped structure (Fig. 4B), whereas in BSF cells, YFP–TbPIPKA appeared in a more rounded form (Fig. 4C). YFP–TbPIPKA did not overlap with labeling with rhodamine–concanavalin-A (ConA, which labels the flagellar pocket) but did localize next to the flagellar pocket, towards the anterior end (Fig. 4Ba,Ca). YFP–TbPIPKA localization did partially overlap with the TbMORN1-labeled arm of the bilobe (Fig. 4Bb,Cb) and was found adjacent to the TbCentrin4 subdomain of the bilobe in PCF and BSF cells (Fig. 4Bc,Cc). Furthermore, YFP–TbPIPKA did not overlap with the flagellar pocket collar that was labeled for TbBILBO1 (Fig. 4Bd,Cd) and was detected next to the posterior tip of the flagellum attachment zone in PCF (Fig. 4Be) and BSF cells (Fig. 4Ce).

Taken together, these results suggest that YFP–TbPIPKA is, mostly, located close to the TbMORN1 subdomain of the bilobe and near to the posterior tip of the flagellum attachment zone.

Journal of Cell Science (2014) 127, 2351–2364 doi:10.1242/jcs.146894

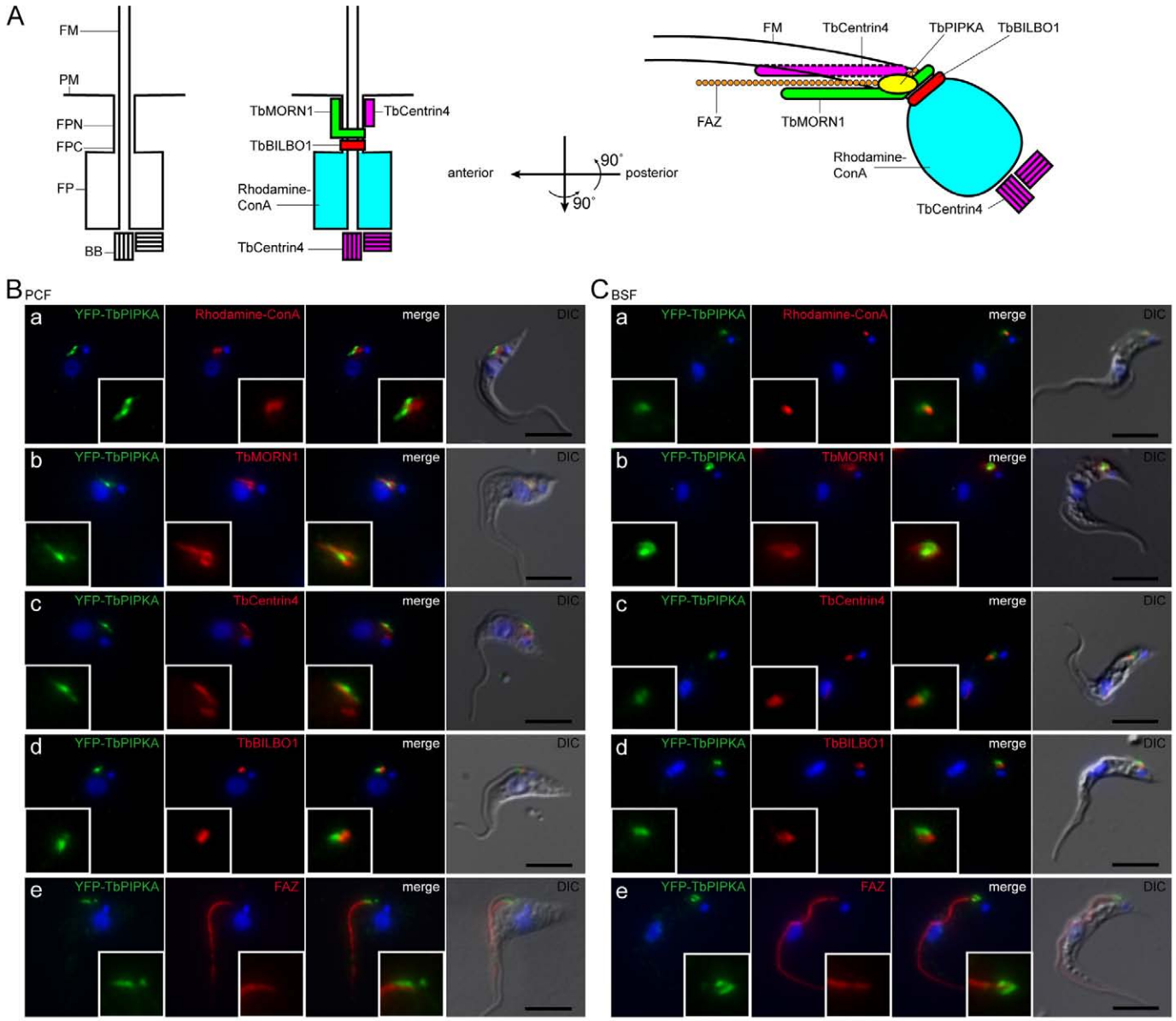

Fig. 4. TbPIPKA localization in PCF and BSF cells. (A) Schematic representation (not to scale) of the flagellar neck region showing the location of marker proteins and TbPIPKA. Top view, left: A single flagellum, surrounded by its own flagellar membrane (FM), nucleates from the basal body (BB) and exits the cell body through the flagellar pocket (FP) at a site termed the flagellar pocket collar (FPC). The plasma membrane (PM) subdomain between the flagellar pocket and that part of the plasma membrane exposed to the environment is termed the flagellar pocket neck (FPN). Top view, middle and right: TbBILBO1 localizes to the flagellar pocket collar. The two arms of the bilobe are labeled by TbMORN1 and TbCentrin4, respectively. TbCentrin4 also localizes to the basal bodies. The flagellar pocket can be labeled with tetramethylrhodamine–Concanavalin A (rhodamine–ConA). Top view, right: The flagellar attachment zone (FAZ) tracks the long axis of the flagellum. (B) PCF cells and (C) BSF cells stably expressing YFP–TbPIPKA from its endogenous promoter. YFP–TbPIPKA was labeled using antibodies against GFP. (a–e) Cells were co-labeled with (a) rhodamine–ConA or antibodies against (b) TbMORN1, (c) TbCentrin4, (d) TbBILBO1 or (e) the FAZ-specific monoclonal antibody L3B2. Nuclear and kinetoplast DNA was labeled with DAPI (blue). Right column in each panel: fluorescence images from the areas indicated were superimposed on differential interference contrast (DIC) images. YFP–TbPIPKA appears to localize to the flagellar pocket neck region, mostly posterior to TbCentrin4, above TbBILBO1 and at the tip of the FAZ. Immunofluorescence images are compressed z-stacks. Scale bars: 5 μm.

PI(4,5)P_2 localizes to the flagellar pocket

Having determined the location of TbPIPKA, we next established the subcellular distribution of its product PI(4,5)P_2. The PH domain of PLCδ binds specifically, and with high affinity, to PI(4,5)P_2 (Lemmon et al., 1995) and a fusion protein of green fluorescent protein with the PH domain of PLCδ ($PH^{PLC\delta}$) has been successfully used to detect PI(4,5)P_2 in living mammalian cells (Stauffer et al., 1998; Várnai and Balla, 1998). A dimer of the $PH^{PLC\delta}$ ($2xPH^{PLC\delta}$) domain fused to GFP has been shown to bind with even higher affinity to this phosphoinositide (Levine and Munro, 2002). Therefore, a YFP–$2xPH^{PLC\delta}$ fusion protein was stably expressed from the constitutively active PARP promoter in PCF cells. YFP–$2xPH^{PLC\delta}$ localized predominantly to a ring-like structure in living cells (Fig. 5A), which was shown to be the flagellar pocket after fixation and co-labeling with rhodamine–ConA, a stain of the flagellar pocket. A YFP–$2xPH^{PLC\delta}$ signal

Journal of Cell Science (2014) 127, 2351–2364 doi:10.1242/jcs.146894

surrounded the rhodamine–ConA-labeling, suggesting that the majority of PI(4,5)P_2 in *T. brucei* is localized to the flagellar pocket membrane (Fig. 5B). The increased cytoplasmic pool of YFP–2xPH$^{PLC\delta}$ was probably an artifact of PFA fixation. This restricted localization to the flagellar pocket membrane was a surprising observation because, in all other studies, PI(4,5)P_2 has been found throughout the plasma membrane (Di Paolo and De Camilli, 2006; Levine and Munro, 2002). It was, therefore, important to confirm the localization at the ultrastructural level; hence, control cells and cells expressing YFP–2xPH$^{PLC\delta}$ were subjected to labeling with immunogold (using an antibody against GFP). In sections of control cells, no gold particles above the background level were detected. By contrast, cells that stably expressed YFP–2xPH$^{PLC\delta}$ displayed strong labeling of the flagellar pocket membrane with very few, if any, gold particles that were at the plasma membrane and exposed to the surrounding medium.

Similar experiments were carried out using BSF cells that stably expressed YFP–2xPH$^{PLC\delta}$. However, these were not viable and an inducible version of the same cells yielded only low levels of YFP–2xPH^{PLC}, too low for detection by fluorescence microscopy.

Interestingly, whereas PI(4,5)P2 localized to the flagellar pocket, the kinase appeared in a punctate structure close to the flagellar pocket. Double-label experiments were used to confirm

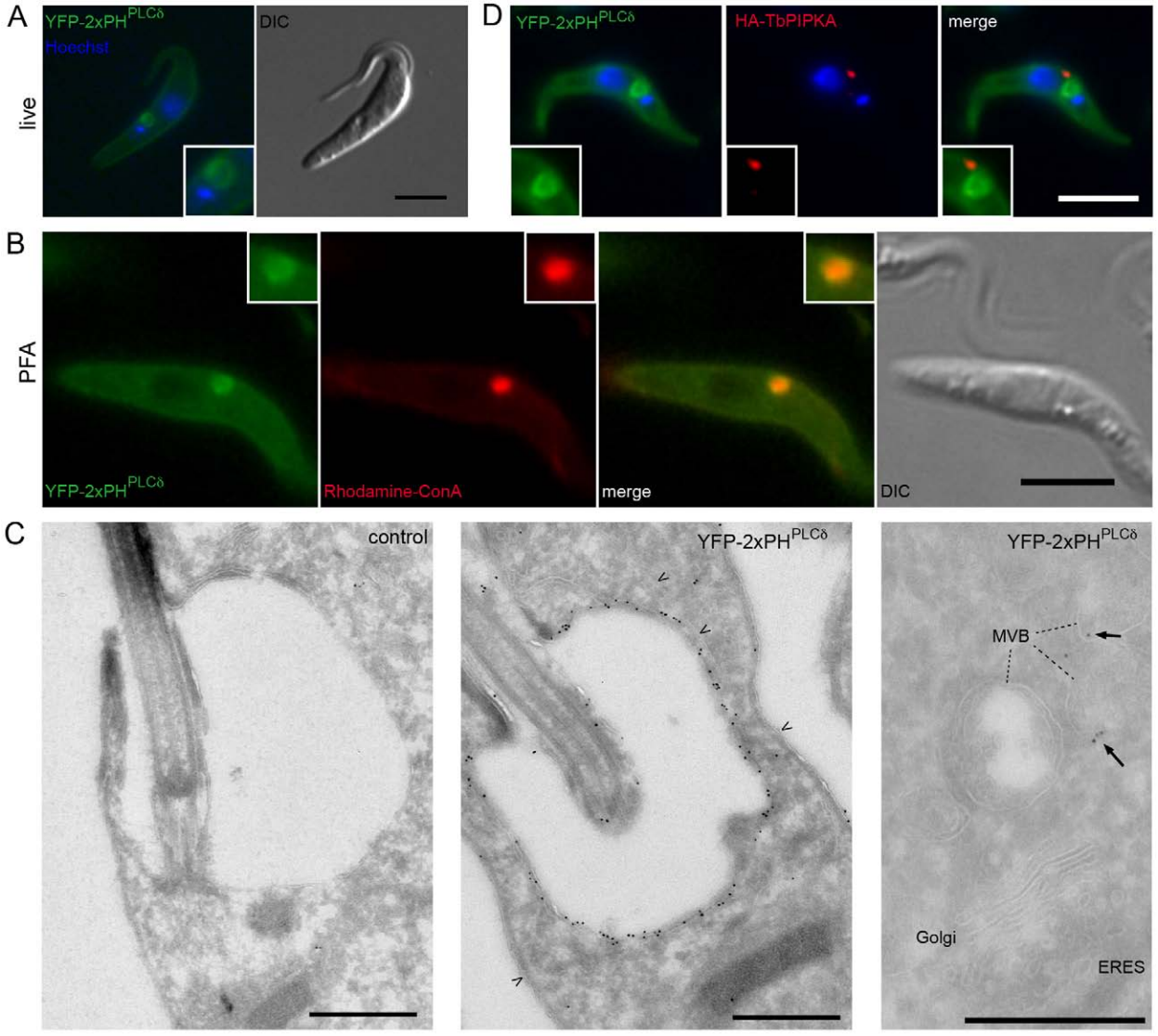

Fig. 5. Distribution of PI(4,5)P_2 using YFP–2xPH$^{PLC\delta}$ as a sensor. (A–C) PCF cells were stably transfected with YFP–2xPH$^{PLC\delta}$ under the control of the strong constitutive PARP promoter. (A) Cells were incubated with 3 μg/ml Hoechst stain (blue) for 25 minutes and imaged live. YFP–2xPH$^{PLC\delta}$ localization (green) was predominantly observed at the flagellar pocket membrane. Some YFP–2xPH$^{PLC\delta}$ was also detected at the plasma membrane. (B) Cells were co-labeled with rhodamine–ConA before fixation. Note that YFP–2xPH$^{PLC\delta}$ localization surrounds the flagellar pocket, as marked by rhodamine–ConA. Note the apparent diffusion of YFP–2xPH$^{PLC\delta}$ in fixed cells relative to living cells. (C) Cryosections of control cells and cells that had been stably transfected with YFP–2xPH$^{PLC\delta}$. Sections were labeled with antibodies against GFP (10-nm gold). Note the labeling of the flagellar pocket membrane, and the absence of labeling over the ER or plasma membrane (arrowheads, middle panel). The right-hand panel shows that PI(4,5)P2 is not present at the ER exit site (ERES) and Golgi. Labeling of multivesicular bodies (MVBs) was variable (dashed lines). Arrows in the right-hand panel indicate gold particles marking the position of YFP–2xPH$^{PLC\delta}$. (D) PCF cells stably expressing HA–TbPIPKA from its endogenous promoter and YFP–2xPH$^{PLC\delta}$ from the PARP promoter, labeled after fixation by using an antibody against HA. Note that TbPIPKA is anterior to the YFP–2xPH$^{PLC\delta}$-labeled pocket. Nuclear and kinetoplast DNA was labeled with DAPI (blue). Scale bars: 5 μm (A,B,D); 500 nm (C).

this, using a cell line that not only stably expressed YFP–2xPH$^{PLC\delta}$ but also an endogenous replacement of TbPIPKA with a hemagglutinin tag (HA–TbPIPKA). As before, the majority of PI(4,5)P_2 was found at the flagellar pocket, and the location of HA–TbPIPKA resembled that previously observed using YFP–TbPIPKA (compare Fig. 4B and Fig. 5D). Furthermore, the kinase did not colocalize with YFP–2xPH$^{PLC\delta}$ (Fig. 5D). HA–TbPIPKA was consistently detected at the anterior neck region, close to the YFP-2xPH$^{PLC\delta}$-labeled flagellar pocket. Ultrastructural localization of TbPIPKA using either the YFP or HA tag did not yield reproducible results, possibly caused by low expression levels.

Localization of YFP–2xPH$^{PLC\delta}$ to the flagellar pocket depends on TbPIPKA

Because TbPIPKA and PI(4,5)P_2 did not colocalize, the requirement of TbPIPKA to localize YFP–2xPH$^{PLC\delta}$ to the flagellar pocket was investigated. Procyclic TbPIPKA-RNAi cells, which had been stably transfected with YFP–2xPH$^{PLC\delta}$, were depleted of TbPIPKA for 3 days and then processed for labeling with immunogold using antibodies against GFP, followed by 10-nm gold (coupled to goat anti-rabbit-IgG antibodies). Induction of RNAi against TbPIPKA resulted in decreased labeling of the flagellar pocket membrane (Fig. 6A,B). The number of gold particles per flagellar pocket from 73 control and 73 RNAi cells was counted. The median number decreased by 78% from 9 to 2 gold particles upon depletion of TbPIPKA (Fig. 6C). By contrast, the circumference of the flagellar pocket profiles in TbPIPKA-depleted cells increased both visually (Fig. 6A,B) and quantifiably (a 14% increase from 3.0 µm to 3.4 µm, Fig. 6D) – the distribution of the circumference profiles from the median was much broader than controls. This probably reflects the variation in the efficiency of RNAi from cell to cell. When both data sets were combined, the labeling density (Fig. 6E) was found to decrease further, by 81% (from 26 to 5.5 gold particles per µm).

Depletion of TbPIPKA enlarges the flagellar pocket volume in PCF and BSF cells

Because TbPIPKA RNAi caused an increase in the median circumference of the flagellar pocket profiles, this suggested that there was a concomitant increase in the volume of the flagellar pocket. To test this, three-dimensional images of the flagellar pocket were generated using serial block-face scanning electron microscopy (serial block-face SEM, SBEM) (Denk and Horstmann, 2004).

PCF cells were induced to express TbPIPKA RNAi for three days and then sectioned. Stacks of 300 slices, from control and TbPIPKA-depleted cells, were imaged. For each slice, the circumference of the flagellar pocket was outlined (Fig. 7A,B) using IMOD 3Dmod software. Forty-five flagellar pockets from control, and 57 flagellar pockets from induced TbPIPKA-RNAi, cells were modeled (Fig. 7C,D). The enlarged volume of the flagellar pockets in TbPIPKA-depleted cells was clearly seen by visual inspection of the reconstructed stacks (Fig. 7B). The calculated mean flagellar pocket volume increased approximately threefold from 1.5×10^{-4} µm^3 in control cells to 5.3×10^{-4} µm^3 in TbPIPKA-depleted cells (Fig. 7E).

The flagellar pocket volume was also measured in BSF TbPIPKA-RNAi cells. Across a stack of 600 slices, 115 flagellar pockets from control cells were modeled (Fig. 7F,H). Three stacks of 600, 300 and 200 slices were analyzed to quantify a total of 158 flagellar pockets from TbPIPKA-depleted cells (Fig. 7G,I; only one stack is shown). As observed in PCF cells, BSF cells showed an approximately threefold increase in the mean flagellar pocket volume (from 4.5×10^{-4} µm^3 to 13×10^{-4} µm^3). However, this threefold increase included a number of outliers (nine cells; 6% of the total) that had extremely large flagellar pockets ($>1.5\times10^{-3}$ µm^3; data not shown). When these nine cells were removed from the quantification to allow statistical testing, the mean value of the flagellar pocket volume of TbPIPKA-depleted cells decreased to 5.8×10^{-4} µm^3, representing a 29% increase (Fig. 7J).

These data show that depletion of TbPIPKA in PCF and BSF cells caused an increase in flagellar pocket size. As seen in cryosections, it was noticeable that, under control conditions, the measured flagellar pocket volumes were narrowly distributed around the median, whereas, in TbPIPKA-depleted cells (Fig. 7E,J), the measured flagellar pocket volumes were more broadly scattered, suggesting that this reflects variations in the RNAi efficiency in each cell.

TbPIPKA depletion causes defects in endocytosis but not export in BSF cells

Because the flagellar pocket is the sole site of endo- and exocytosis in *T. brucei*, an increase in flagellar pocket volume could be explained by an imbalance between these two processes. If the rate of export increases, or endocytosis is inhibited [through depletion of PI(4,5)P_2], then the flagellar pocket should get bigger. This has been described previously in clathrin-RNAi cells as the big-eye phenotype, a consequence of decreased endocytosis (Allen et al., 2003). To test this hypothesis, TbPIPKA was depleted using RNAi in BSF cells for 3 days, and the cells were assayed for endocytosis and export.

Because trypanosomes take up iron using transferrin and transferrin receptors (Steverding, 2000), receptor-mediated endocytosis of transferrin that had been labelled with Alexa Fluor 633 (AF633) was analyzed by fluorescence-activated cell sorting (FACS), allowing quantification of a large number of cells. Depletion of TbPIPKA led to a 30% reduction in AF633–transferrin endocytosis (Fig. 8A). Interestingly, inducible ectopic overexpression of Ty1–TbPIPKA did not change the rate of AF633–transferrin endocytosis (data not shown), suggesting that the endogenous levels of TbPIPKA [hence PI(4,5)P_2] are not limiting for endocytosis. To investigate the rate of export in BSF cells, VSG was used as a tool. VSG is a glycosylphosphatidylinositol (GPI)-anchored protein and the major secretory cargo in *T. brucei* (Grünfelder et al., 2002; Jackson et al., 1985). VSG is assembled in the endoplasmic reticulum (ER), transported through the Golgi to the flagellar pocket membrane – either directly or through endosomes (Bangs et al., 1986; Bangs et al., 1985; Duszenko et al., 1988; Ferguson et al., 1986). VSG at the cell surface is susceptible to cleavage by an endogenous phospholipase (GPI-PLC) after hypotonic cell lysis. Intracellular VSG is inaccessible and so is not cleaved.

BSF cells were depleted of TbPIPKA for 3 days, and newly synthesized proteins were pulse-labeled for up to 45 minutes using [^{35}S]methionine-cysteine. Surface and internal VSG were recovered using ConA–Sepharose beads. In control cells, the half-time of VSG secretion was ~8 minutes and this was not changed substantially upon depletion of TbPIPKA (Fig. 8B). Taken together with the endocytic data, this suggests that the increase in the size of the flagellar pocket was caused by a decrease in the rate of endocytosis, not a change in the rate of export.

Journal of Cell Science (2014) 127, 2351–2364 doi:10.1242/jcs.146894

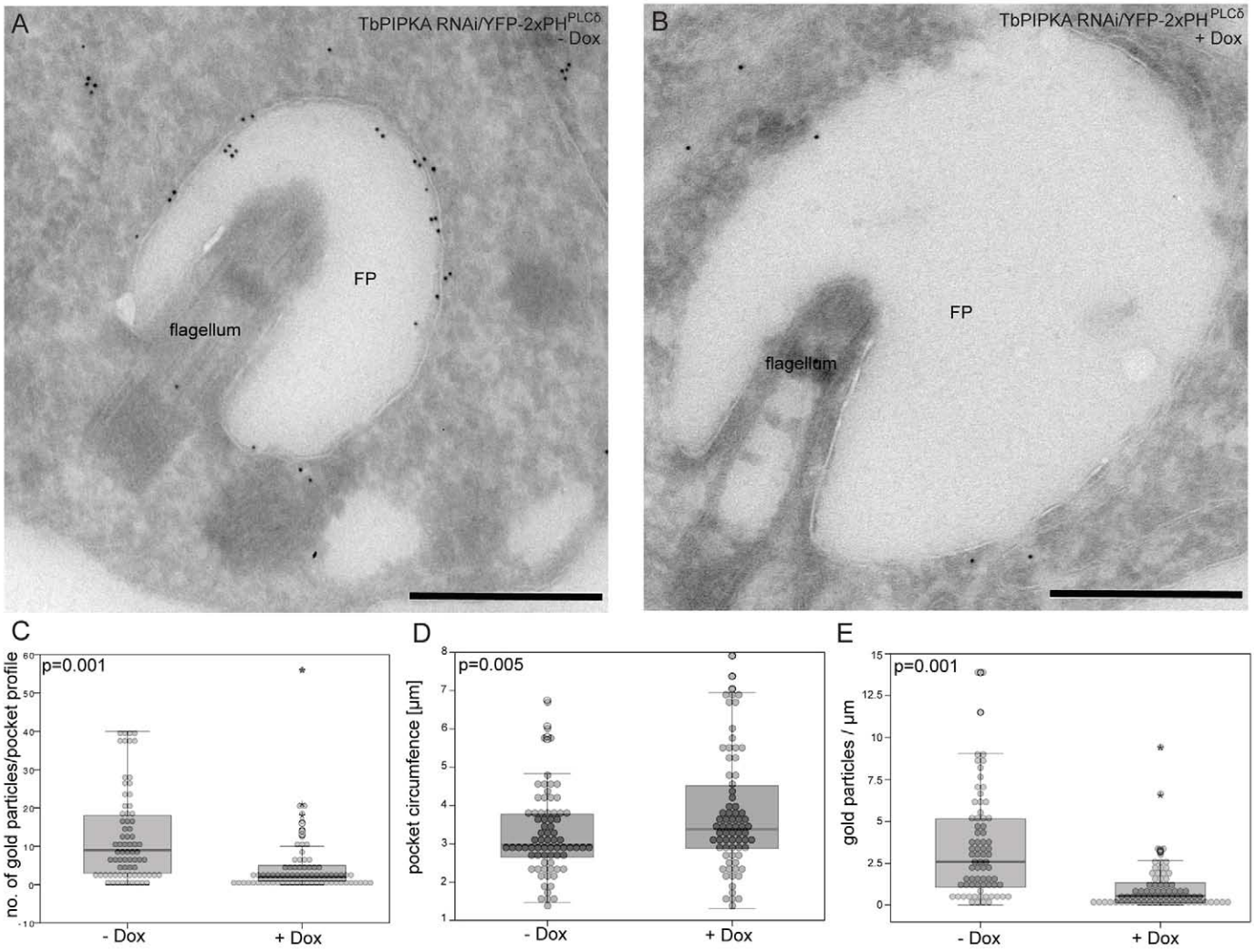

Fig. 6. Depletion of TbPIPKA alters the levels of PI(4,5)P_2 at the flagellar pocket. (A,B) TbPIPKA-RNAi cells were stably transfected with YFP–2xPH$^{PLC\delta}$ expressed under the control of the PARP promoter. TbPIPKA depletion was induced for 3 days (+Dox). Cryosections of control (−Dox; left hand panel) and induced (+Dox; right hand panel) cells were labeled with antibodies against GFP (10-nm gold). FP: flagellar pocket. Scale bars: 500 nm. (C–E) Flagellar pocket profiles from control (n=73) and TbPIPKA-depleted (n=73) cells were analyzed. Statistical significance (P-values) is indicated in the histograms. The box represents the 25th–75th percentiles, the line represents the median and the whiskers encompass 95% of the data points. (C) The number of gold particles per flagellar pocket profile was counted manually. (D) The circumference of flagellar pocket profiles was measured using ImageJ software. Depletion of TbPIPKA led to a small, but statistically significant, increase in the number of cells that had enlarged flagellar pockets. (E) The ratio of gold particles:circumference (µm) was plotted. A strong decrease in the linear density (gold particles/µm) of the labelling of YFP–2xPH$^{PLC\delta}$ at the flagellar pocket was observed.

DISCUSSION

Here we have provided several lines of evidence showing that Tb927.10.1620 mediates PI(4,5)P_2 synthesis. Tb427.04.1620 shares a high level of sequence identity and similarity with known mammalian and yeast PIP kinases. Though annotated in the database as a type II PIP kinase, Tb927.10.1620 has a short amino acid stretch in the activation loop that is found in type I enzymes, suggesting that it is a PI4P 5-kinase (Doughman et al., 2003; Kunz et al., 2000). Depletion of this enzyme led to a lower PIP_2:PIP ratio, which would be expected to reflect the PI(4,5)P2:PI4P ratio, as these two phosphoinositides represent the most abundant PIP2 and PIP species. In agreement with this, depletion of Tb427.04.1620 resulted in the decreased recruitment of YFP–2xPH$^{PLC\delta}$, a PI(4,5)P_2 reporter, to the flagellar pocket membrane. Conversely, overexpression of Tb427.04.1620 resulted in increased amounts of PIP_2 and reduced levels of PIP. So far, we have not been able to show directly that this protein converts PI4P to PI(4,5)P_2 because expression in *Escherichia coli* leads to an insoluble product. Additionally, immune-precipitation from cell extracts did not yield a protein that was sufficiently active for enzymatic analysis. Hence, although our data strongly suggest that Tb427.04.1620 is a PI4P 5-kinase, further work is needed to confirm this. For this reason we have termed Tb427.04.1620 as TbPIPKA throughout the paper, the suffix ‘A’ denoting the fact that there are two other other putative PIP kinases in the trypanosome database.

TbPIPKA is essential for the growth of PCF and BSF cells. Because depletion of TbPIPKA was not accompanied by changes in the distribution of the different cell-cycle stages, this suggests alteration of a process (or processes) that is constitutively needed throughout the cell cycle. For example, a lack of PI(4,5)P_2 interfering with nutrient uptake, which is mediated by endocytosis in *T. brucei*. The fact that transferrin uptake in BSF cells was reduced by 30% upon depletion of TbPIPKA is

Journal of Cell Science (2014) 127, 2351–2364 doi:10.1242/jcs.146894

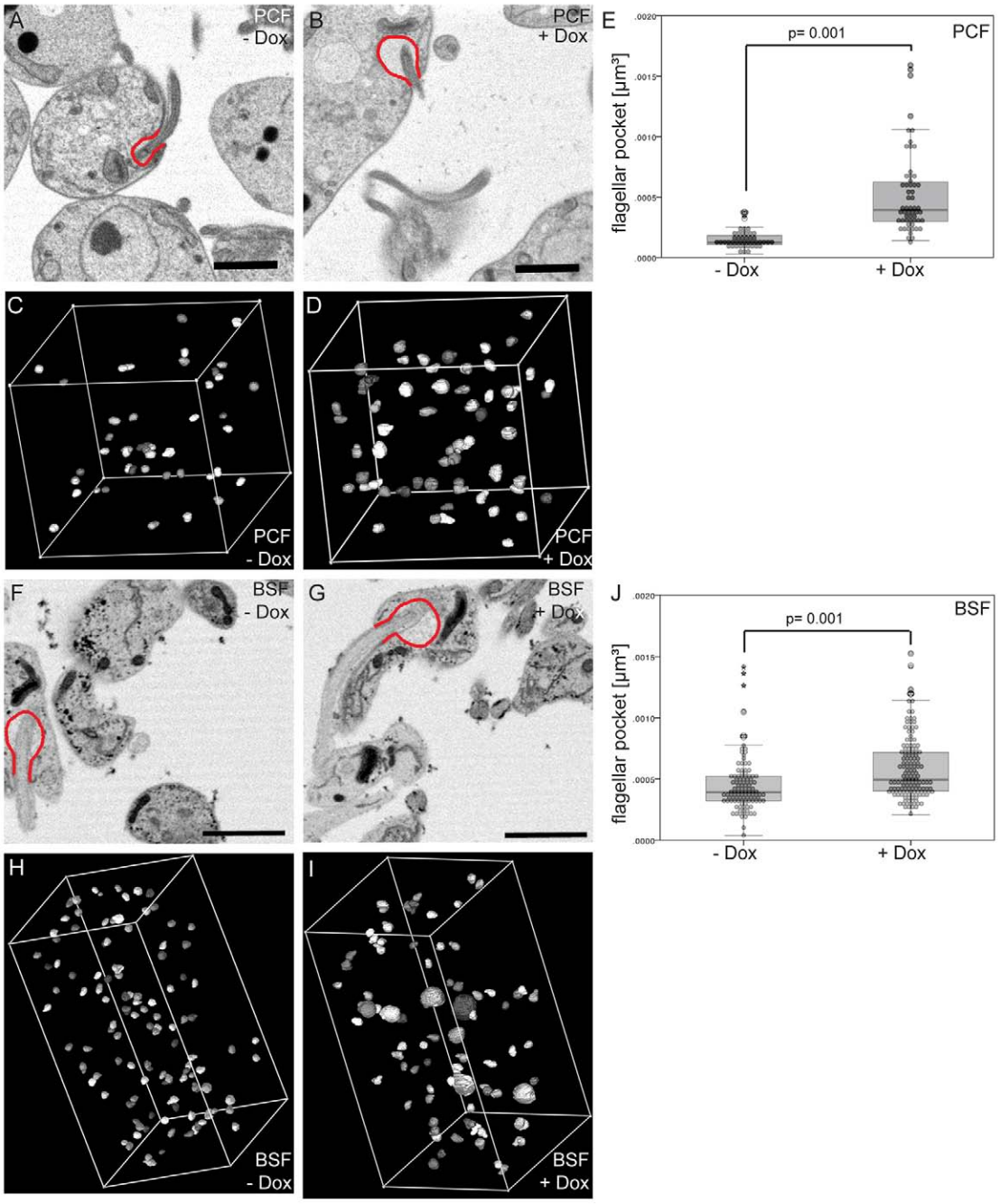

Fig. 7. Depletion of TbPIPKA causes an increase in flagellar pocket volume. (A–E) PCF and (F–J) BSF TbPIPKA-RNAi cells were induced for 3 days and analyzed by serial block-face scanning electron microscopy. Single slices of (A) control (–Dox) and (B) induced (+Dox) PCF cells are shown. To estimate the enlargement of the flagellar pocket, a representative flagellar pocket in each reconstruction was outlined in red. The flagellar pocket circumference was tracked using the IMOD 3Dmod software in 300 acquired sections: 45 flagellar pockets from control cells (C) and 57 flagellar pockets from TbPIPKA-depleted cells (D) were modeled. (E) The volume of the flagellar pockets was calculated using 3Dmod software and plotted as a histogram. Single slices of control (F) and induced (G) BSF cells are shown. The flagellar pocket volumes of 115 control cells (H) and 158 TbPIPKA-depleted cells (I), from a total of 1700 sections, were modeled and plotted as a histogram. (J) 6% of TbPIPKA-depleted cells with extremely large flagellar pocket (nine cells) were removed from the data set and the remaining values plotted as a histogram. Scale bars: 2 µm.

consistent with this explanation. More puzzling is the evidence that depletion of TbPIPKA slows growth equally in both PCF and BSF cells, despite the much higher rate of endocytosis in BSF cells. The simplest explanation is that one, or both, of the two other putative PIP kinases that have been identified in trypanosomes are involved and can compensate for the loss of TbPIPKA to differing extents in the two parasite forms.

The inhibition of transferrin uptake in BSF cells was accompanied by an increase in the size of the flagellar pocket, most probably the consequence of an imbalance in membrane trafficking pathways. Export of VSG was not affected by depletion of TbPIPKA, suggesting that more membrane is added to the flagellar pocket than is removed by endocytosis, resulting in an increase in size. The source of this additional

Journal of Cell Science (2014) 127, 2351–2364 doi:10.1242/jcs.146894

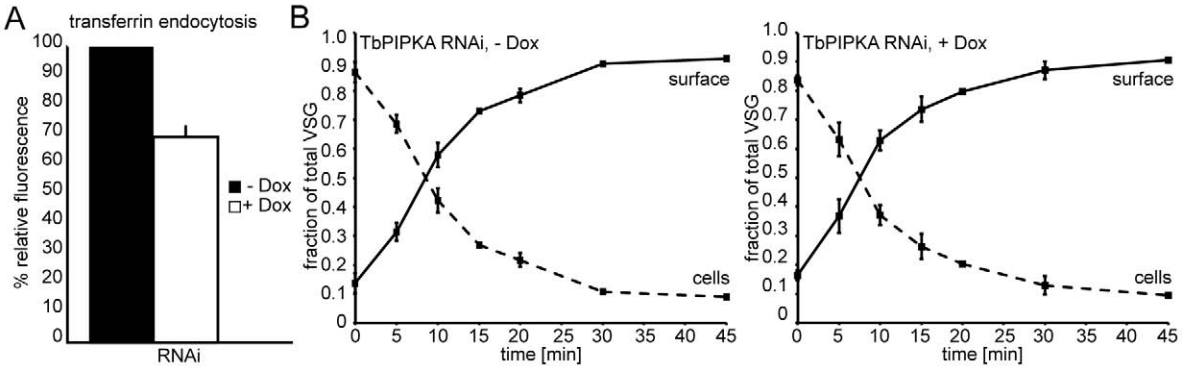

Fig. 8. TbPIPKA depletion negatively affects endocytosis but not export. (A) Endocytosis of AF633–transferrin in BSF cells. TbPIPKA-RNAi was induced for three days. The ligand uptake was calculated by determining the relative fluorescence mean values of the FACS data. The relative fluorescence values for control cells (−Dox) were set to 100% and the fluorescence values for the depleted cells (+Dox) were normalized to these values. Six independent RNAi experiments were performed. The values shown are mean±s.e.m. The induction of TbPIPKA-RNAi resulted in a reduced rate of receptor-mediated endocytosis of transferrin. (B) Export of VSG in BSF cells. Radiolabeled surface and internal VSG was recovered using ConA–Sepharose beads. The data were compiled from three independent experiments; the values shown are the mean±s.e.m. The depletion of TbPIPKA (right panel) did not significantly affect the half-time for VSG delivery to the cell surface.

membrane could be either post-trans-Golgi-network vesicles or endosomes (Futter et al., 1995; Griffiths and Simons, 1986; Taguchi, 2013). This increase in the size of the flagellar pocket upon depletion of TbPIPKA was much less pronounced than the so-called big-eye phenotype that has been described upon the inhibition of endocytosis by depletion of clathrin or actin (Allen et al., 2003; García-Salcedo et al., 2004). This might also help to explain why there was no change in the distribution of the cell-cycle stages after depletion of TbPIPKA, because the increase in the size of the flagellar pocket might be insufficient to disrupt processes, such as cytokinesis, that are severely affected in the big-eye phenotype.

The increase in the size of the flagellar pocket differed between PCF and BSF cells. For PCF cells, there was a threefold increase upon depletion of TbPIPKA; for BSF cells, the increase was 1.3-fold (excluding outliers). This did not correlate with the remaining levels of TbPIPKA, because PCF cells had more than BSF cells. PI(4,5)P_2 is a crucial requirement for endocytosis in all other organisms studied to date, suggesting that, here, either the knockdown was insufficient or that one, or both, of the other two putative kinases that were identified by the bioinformatics analysis might be able to compensate for the loss of TbPIPKA. Further work on these putative PIP kinases will be necessary to address this, and earlier, points.

It was surprising that TbPIPKA was not localized to the flagellar pocket, where the product PI(4,5)P_2 was found, instead, it localized adjacent and anterior to the neck region. TbPIPKA was always found at a spot adjacent to the flagellar pocket collar marker TbBILBO1 and exhibited the most prominent overlap with the hook-like staining of TbMORN1 (a component of the bilobe; Esson et al., 2012). It does not, however, precisely overlap with any known morphological feature in this region. The resolution of light-microscopy is too low; therefore, further work using immuno-electron microscopy will be needed to draw any further conclusions.

PI4P, which is the substrate for PI4P 5-kinases at the plasma membrane is generated by the enzyme Stt4 (in yeast) and PI4KIIIα (in mammals). There does not, however, appear to be an equivalent homologue in trypanosomes. The main pool of PI4P is present at the Golgi in *T. brucei* (our unpublished data; Levine and Munro, 2002); therefore, it is not in the immediate vicinity of the enzyme. Access could be achieved either by bringing the kinase to the substrate or the substrate to the kinase. Sac1, a phosphatase involved in PIP metabolism, can shuttle between the ER and the Golgi (Faulhammer et al., 2007) and also act at membrane contact sites between the ER and plasma membrane (Stefan et al., 2011). Conceivably, a fraction of TbPIPKA could also be mobile. Alternatively, and perhaps more likely, PI4P could be delivered to the kinase at the neck of the flagellar pocket, possibly by vesicular transport. Post-Golgi (or endosomal) transport vesicles deliver their cargo to the flagellar pocket, but it is unknown whether delivery can occur anywhere on the flagellar pocket. Perhaps specialized domains exist, and transport vesicles containing PI4P can be preferentially delivered to the neck of the flagellar pocket where TbPIPKA is located. Because the exocyst marks the delivery site of post-Golgi vesicles from yeast to mammals (Guo et al., 1999; TerBush et al., 1996; Wang and Hsu, 2006), it would be interesting to localize one or more of its subunits. If it is located at the neck, and below the collar, then it would be a simple matter for the product [PI(4,5)P_2] to reach the flagellar pocket and diffuse rapidly throughout the pocket. More surprising is the fact that PI(4,5)P_2 does not then exit the flagellar pocket and diffuse throughout the plasma membrane. This suggests the existence of a ‘fence’ that prevents phosphoinositide diffusion from the neck region to the rest of the plasma membrane. In all other organisms, this phosphoinositide is present throughout the plasma membrane – there are no domains in which it is enriched.

But what are the effectors of PI(4,5)P_2 at the flagellar pocket membrane in clathrin-mediated endocytosis in trypanosomes? The only clathrin adaptor described, to date, in trypanosomes that might have the ability to bind to phosphoinositides and has a role in endocytosis is the ENTH-domain-containing protein TbEpsinR (Gabernet-Castello et al., 2009), which is thought to function as the homologue of both the epsin-family of proteins (clathrin adaptors that function at the plasma membrane) (De Camilli et al., 2002) and epsinR (a clathrin adaptor that functions in transport between the Golgi complex and endosomes) (Saint-Pol et al., 2004). TbEpsinR localizes to the flagellar pocket and compartments along the early endocytic pathway. It is required for the endocytosis of GPI-

anchored, as well as transmembrane, proteins and it interacts with clathrin, just as the mammalian epsins and epsinR do (Rosenthal et al., 1999; Wasiak et al., 2002). Basic residues that participate in binding to PIPs are well conserved (Gabernet-Castello et al., 2009), but it remains to be determined whether TbEpsinR actually binds to phosphoinositides, especially PI(4,5)P_2, as mammalian epsins do (Ford et al., 2002). In this context, it is interesting to note that depletion of TbPI4KIIIβ which generates PI4P, the substrate for phosphatidyl-inositol 5-kinases, causes enlargement of the flagellar pocket, consistent with an inhibition of endocytosis (Gabernet-Castello et al., 2009). Furthermore, this depletion impairs the association of TbEpsinR with the flagellar pocket membrane, raising the possibility that TbEpsinR might bind to PI(4,5)P_2. However, this is only a correlation, and further work needs to focus on the potential phosphoinositide-binding properties of TbEpsinR, as well as other orthologues that could be involved in the endocytic process in *T. brucei*.

MATERIALS AND METHODS

Cell lines

All experiments using procyclic *T. brucei* (PCF) were performed in 29-13 cells (Wirtz et al., 1999) provided by George Cross (Rockefeller University, NY). Cells were cultured at 27℃ in SDM-79 medium supplemented with 20% heat-inactivated Tet-system-approved fetal calf serum (Clontech), 6.5 µg/ml haemin, 15 µg/ml G418 and 50 µg/ml hygromycin. Experiments with bloodstream-form cells (BSF) were carried out using the MITat 1.2 single-marker line (Wirtz et al., 1999). BSF cells were cultivated at 37℃ under 5% CO_2 in HMI-9 media supplemented with 10% heat-inactivated Tet-system-approved fetal calf serum and 2.5 µg/ml G418.

To generate a stable and inducible Ty1–TbPIPKA-expressing cell line, the Tb927.10.1620 open reading frame was cloned into the pLew100 vector using *Hin*dIII and *Bam*HI. The sequence for the Ty1 tag was incorporated in the forward primer between the *Hin*dIII restriction site and the start of the open reading frame lacking the start codon. The vector was linearized with *Cla*I before transfection into 29-13 or MITat 1.2 single-marker cells.

In order to create a stable and inducible TbPIPKA-RNAi cell line, the nucleotides 610–1086 of Tb927.10.1620 were cloned into pZJM (Wang et al., 2000) using *Xba*I. The specific target sequence was chosen using the RNAit software in GeneDB (http://trypanofan.path.cam.ac.uk/software/RNAit.html) (Redmond et al., 2003). The vector was linearized with *Not*I and transfected into 29-13 cells. The same sequence was cloned using TA-overhangs into $p2T7^{TAblue}$ (Alibu et al., 2005) before being linearized with *Not*I and transfected into the MITat 1.2 single-marker cell line.

The YFP-$2xPH^{PLC\delta}$-pXS2 construct is based on the pTL336 plasmid (Levine and Munro, 2002). $2xPH^{PLC\delta}$ was cloned using *Bam*HI and *Bgl*II into a pXSGFPM3FUS expression vector (Bangs et al., 1996; Marchetti et al., 2000) in which GFP was replaced by YFP. Before transfection, the plasmid was linearized by using *Nsi*I.

One of the TbPIPKA alleles was endogenously replaced with either YFP–TbPIPKA or HA–TbPIPKA. Replacements were generated as previously described (Arhin et al., 2004).

Stably transfected PCF cells were selected using 5 µg/ml phleomycin (pZJM, pLew100), 10 µg/ml blasticidin (pXS2, endogenous replacement) or 2 µg/ml puromycin (endogenous replacement). Clonal cell lines were obtained by serial dilution. BSF cells were stably transfected with an Amaxa Nucleofactor electroporator (program X-001) and human T cell solution (Lonza). Stable clones were selected by using 3 µg/ml blasticidin (endogenous replacement), 3 µg/ml phleomycin (pLew100) or 5 µg/ml hygromycin ($p2T7^{TAblue}$).

Bioinformatics

The alignments were generated by first aligning the yeast ScMss4 protein sequence with the human HsPIPKIα (NP_003548) and HsPIPKIβ (NP_003550) protein sequences using MAFFT (v6.833b; Katoh et al., 2005) with the linsi option. Second, the *T. brucei* sequences were added to the guide alignment, again by using MAFFT. The PI4P 5-kinase Pfam (Punta et al., 2012) domain region of the alignment is shown (ScMss4p, amino acids 438–756; HsPIPKIα, amino acids 124–436; HsPIPKIβ, amino acids 93–415; Tb427.04.1620, amino acids 150–480; Tb427.10.4770, amino acids 90–433; Tb427.10.3890, amino acids 577–890).

Silencing TbPIPKA expression using RNAi

TbPIPKA-RNAi cells (PCF) were seeded at a density of 10^6 cells/ml and cultured in the absence or presence of 5 µg/ml doxycycline at 27℃. Cells were reseeded at 1×10^6 cells/ml with fresh doxycycline every 48 hours. For BSF TbPIPKA-RNAi cells, parallel cultures were initially seeded with 10^5 cells/ml and 1 µg/ml doxycycline was added to one flask to induce the RNAi. Cells were reseeded at 10^5 cells/ml with fresh doxycycline every 48 hours. Cell numbers were quantified using a particle counter (Z2 Coulter Counter; Beckman Coulter) and particles of a size between 3 and 10 µm were counted.

Antibodies

The monoclonal antibody against Ty1 and the FAZ-specific L3B2 monoclonal antibody (Kohl et al., 1999) were generous gifts from Keith Gull (University of Oxford, Oxford, UK). The polyclonal antibody against *Leishmania donovani* centrin 4 was obtained from Hira Nakhasi (US Food and Drug Administration, MD). The polyclonal antibodies against GFP, TbMORN1 and TbBILBO1 have been described previously (Esson et al., 2012; Morriswood et al., 2013; Seedorf et al., 1999). The monoclonal antibody against HA was purchased from Covance Research Products, and the monoclonal antibody against GFP from Roche.

HPLC analysis

Phosphatidylinositol phosphate analysis was performed using a method adapted from C. Nasuhoglu and colleagues, which allows identification of PIP_2 and PIP without radiolabeling (Nasuhoglu et al., 2002). Anionic lipids were extracted from trypanosome pellets with 0.5 ml $CHCl_3$:CH_4O (1:1), 0.5 M HCl, 2 mM $AlCl_3$. After homogenization, 0.4 ml $CHCl_3$ and 0.3 ml 1 M HCl were added. Samples were vigorously mixed and then centrifuged to separate the phases. The organic fraction containing the lipids was removed to a clean tube and dried under nitrogen gas. Lipids were deacetylated and the resuspended head groups were analyzed by HPLC using an anion exchange column and a conductivity detector.

Semi-quantitative RT-PCR

RNA was isolated using Trizol (Invitrogen) according to the manufacturer's instructions. Samples were subjected to reverse-transcriptase (RT)-PCR using the Qiagen OneStep RT-PCR Kit according to the manufacturer's protocol. A fragment of the TbPIPKA open reading frame was amplified by RT-PCR using the primers 5′-CACGTCGCACTCCTACGGAG-3′ and 5′-GTGTGCTGTGCCAGCGGC-3′ (1.5 µg RNA, 31 cycles); a β- tubulin fragment was amplified using the primers 5′-ATGCGCGAAATCGT-CTGCG-3′ and 5′-GACACCTTGGGGGATGGGATGATG-3′ (1.0 µg RNA, 25 cycles). To control for DNA contamination, the β-tubulin fragment was amplified using Taq-polymerase (1.0 µg RNA, 30 cycles).

Concanavalin A labeling

For PCF, 5×10^6 cells were washed three times with PBS. Samples were always spun at 1000 ***g*** for 5 minutes at 4℃. Cells were re-suspended in 1 ml of ice-cold 3% BSA in PBS containing 0.1 M methyl α-D-mannopyranoside, and 30 µg/ml tetramethylrhodamine–concanavalin-A (Molecular Probes) was added. The tube was put on an orbital mixer for 30 minutes at 4℃ in the dark. Subsequently, 1 ml of ice-cold 3% BSA in PBS containing 0.4 M methyl α-D-mannopyranoside was added, and the cells were incubated on an orbital shaker for 30 minutes at 4℃. Then cells were spun, re-suspended in 1 ml of ice-cold 0.2 M Methyl α-D-mannopyranoside in 3% BSA in PBS and incubated on an orbital shaker for 20 minutes at 4℃. Cells were washed three times with 0.2 M methyl α-D-mannopyranoside in 3% BSA in PBS and once with PBS.

Subsequently, cells were spun onto coverslips and fixed with 4% paraformaldehyde (PFA) for 30 minutes. Coverslips were either washed with PBS, mounted and directly analyzed by fluorescence microscopy or further processed for immunofluorescence microscopy.

Labeling of BSF was performed as previously described (Allen et al., 2003) with the exception that all incubations were carried out at 4℃ and cells were spun onto coverslips before fixation with ice-cold 4% PFA for 1 hour.

Immunofluorescence microscopy

PCF cells were washed once with PBS, centrifuged onto a coverslip (1800 ***g***, 1 minute) and fixed with ice-cold methanol (9 minutes, −20℃). BSF cells were washed once with PBS and centrifuged onto poly-L-lysine-coated coverslips (1000 ***g***, 1 minute). Cells were first fixed for 2 minutes with 4% PFA and immediately afterwards with −20℃ cold methanol for another 4 minutes. PCF and BSF samples were rehydrated with PBS and subsequently blocked with 3% BSA in PBS for 45 minutes at room temperature.

Cells (PCF and BSF) that had been labeled with rhodamine–ConA and fixed with 4% PFA were subsequently permeabilized for 4 minutes with 0.25% Triton X-100 in PBS, washed three times with PBS and then blocked with 3% BSA in PBS for 45 minutes at room temperature.

All further steps, including antibody binding, washing steps and mounting have been described previously (Demmel et al., 2011). Images were acquired by using an inverted microscope (Axio Observer Z1, Carl Zeiss MicroImaging Inc.) equipped with a PCO 1600 camera. Image processing was performed using ImageJ and Adobe Photoshop CS5 software (Adobe Systems, San Jose, CA).

Immuno-electron microscopy

Approximately 5×10^8 PCF cells were prepared according Tokuyasu's method (Geuze et al., 1981; Liou et al., 1996). Briefly, cells were fixed with 0.2% glutaraldehyde and 2% paraformaldehyde in phosphate buffer and embedded in 12% gelatin. After cryoprotection in 2.3 M sucrose, 70-nm thick sections were cut by using a Leica EM UC6 ultramicrotome equipped with a Leica EM FCS cryosetup. The YFP-tagged $PH^{PLC\delta}$ domain was labeled with an antibody against GFP (1:300) and followed by detection with an antibody against rabbit IgG coupled to 10-nm gold (BBInternational). Images were acquired using a Morgagni 268D electron microscope (FEI) fitted with a Morada CCD camera (Olympus-SIS). The gold label was counted manually and the flagellar pocket circumference was measured using ImageJ.

Serial block-face SEM

PCF cells were prepared according to published protocols (Schwarz et al., 2000). Preparation of BSF cells followed a protocol modified from Deerinck and colleagues (http://ncmir.ucsd.edu/sbfsem-protocol.pdf). SBEM measurements (Denk and Horstmann, 2004) were performed by using a FEI ESEM Quanta 600 FEG (FEI, Eindhoven, The Netherlands) and a prototype *in situ* ultramicrotome from Gatan (Pleasanton, CA). The energy of the primary electrons was 4 keV using backscattered electrons for imaging in the low vacuum mode of the environmental scanning electron microscope (ESEM). Low vacuum was established by water vapour at a pressure of about 120 Pa. Sample blocks were cut into small cuboids of about $0.5\times0.5\times0.5$ mm^3 and fixed on special rivets (Zankel et al., 2009). A slice thickness of 80 nm and a pixel resolution of 1024×1024 at an image width of 25 µm resulted in a voxel size of $25\times25\times80$ nm^3. Flagellar pockets were outlined as in Fig. 7A,B,F,G and, additionally, closed at the flagellar pocket necks. The volumes of these closed objects were calculated in IMOD 3Dmod software (Kremer et al., 1996). Data were transferred to Microsoft Excel and SPSS for statistical evaluation.

Statistical analysis of electron-microscopy images

Statistical analyses were performed by using Welch's T-Test. Graphs were plotted with the SPSS Statistics package (IBM, version 21) and shown as an overlay of 2D dot plots and box plots from the same datasets.

Transferrin-uptake assay

Receptor-mediated endocytosis of AF633-transferrin was performed as described previously (Gabernet-Castello et al., 2009). A total of 50,000–60,000 cells was analyzed and fluorescence was measured using the FACSCalibur instrument (BD Biosciences). Data were analyzed by using the FlowJo software.

VSG export assay

Export of VSG was followed as described previously (Allen et al., 2003) with some modifications. After three days of RNAi, BSF cells were maintained for 15 minutes in cysteine-methionine-free medium, pulse-labeled with [^{35}S]methionine (50 µCi/ml EXPRE^{35}S^{35}S protein labeling mix; Perkin Elmer) for 2 minutes and then samples were taken at the indicated chase times. Surface VSG was released using the activity of the endogenous GPI-PLC; the intracellular pool of VSG was solubilized using cell lysis. VSG was then precipitated using 25 µl of a 50% ConA–Sepharose-4B bead slurry (GE Healthcare). After retrieval of VSG and subsequent washes, beads were re-suspended in 50 µl 2×SDS-loading buffer. Proteins were fractionated using SDS-PAGE in 10% gels and the dried gel was exposed to an imaging plate (Raytest). Imaging plates were scanned using a Typhoon 8600 variable scanner (Molecular Dynamics) and the amounts of VSG quantified using ImageJ software.

Acknowledgements

We thank Brooke Morriswood and Sevil Yavuz (MFPL, Vienna, Austria) for critical reading of the manuscript. We are grateful to Claudia Mayrhofer (Institute for Electron Microscopy, Graz, Austria) for technical assistance with the SBEM preparation. We are also indebted to Günter Resch (CSF EM facility IMBA, Vienna, Austria) for generating 3D volumes from SBEM images and technical help with the 3Dmod software. We are further thankful to all past and present members of the Warren laboratory for discussions and sharing reagents.

Competing interests

The authors declare no competing interests.

Author contributions

L.D., K.S., G.W. and P.d.C. conceived the experiments; L.D., K.S., L.L., K.H., A.Z., T.K. and V.R. conducted the experiments; and G.W., L.D., K.S. and P.d.C. wrote the manuscript.

Funding

This work was funded by the University of Vienna and the Medical University of Vienna. This work was supported, in part, by grants from the National Institutes of Health to Pietro de Camilli [grant numbers R37NS036251-14 and DK082700]. Deposited in PMC for release after 12 months.

Supplementary material

Supplementary material available online at
http://jcs.biologists.org/lookup/suppl/doi:10.1242/jcs.146894/-/DC1

References

Achiriloaie, M., Barylko, B. and Albanesi, J. P. (1999). Essential role of the dynamin pleckstrin homology domain in receptor-mediated endocytosis. *Mol. Cell. Biol.* **19**, 1410-1415.

Alibu, V. P., Storm, L., Haile, S., Clayton, C. and Horn, D. (2005). A doubly inducible system for RNA interference and rapid RNAi plasmid construction in Trypanosoma brucei. *Mol. Biochem. Parasitol.* **139**, 75-82.

Allen, C. L., Goulding, D. and Field, M. C. (2003). Clathrin-mediated endocytosis is essential in Trypanosoma brucei. *EMBO J.* **22**, 4991-5002.

Arhin, G. K., Shen, S., Ullu, E. and Tschudi, C. (2004). A PCR-based method for gene deletion and protein tagging in Trypanosoma brucei. *Methods Mol. Biol.* **270**, 277-286.

Aslett, M., Aurrecoechea, C., Berriman, M., Brestelli, J., Brunk, B. P., Carrington, M., Depledge, D. P., Fischer, S., Gajria, B., Gao, X. et al. (2010). TriTrypDB: a functional genomic resource for the Trypanosomatidae. *Nucleic Acids Res.* **38**, D457-D462.

Bangs, J. D., Hereld, D., Krakow, J. L., Hart, G. W. and Englund, P. T. (1985). Rapid processing of the carboxyl terminus of a trypanosome variant surface glycoprotein. *Proc. Natl. Acad. Sci. USA* **82**, 3207-3211.

Bangs, J. D., Andrews, N. W., Hart, G. W. and Englund, P. T. (1986). Posttranslational modification and intracellular transport of a trypanosome variant surface glycoprotein. *J. Cell Biol.* **103**, 255-263.

Bangs, J. D., Brouch, E. M., Ransom, D. M. and Roggy, J. L. (1996). A soluble secretory reporter system in Trypanosoma brucei. Studies on endoplasmic reticulum targeting. *J. Biol. Chem.* **271**, 18387-18393.

Bastin, P., Pullen, T. J., Moreira-Leite, F. F. and Gull, K. (2000). Inside and outside of the trypanosome flagellum:a multifunctional organelle. *Microbes Infect.* **2**, 1865-1874.
Berriman, M., Ghedin, E., Hertz-Fowler, C., Blandin, G., Renauld, H., Bartholomeu, D. C., Lennard, N. J., Caler, E., Hamlin, N. E., Haas, B. et al. (2005). The genome of the African trypanosome Trypanosoma brucei. *Science* **309**, 416-422.
Bonhivers, M., Nowacki, S., Landrein, N. and Robinson, D. R. (2008). Biogenesis of the trypanosome endo-exocytotic organelle is cytoskeleton mediated. *PLoS Biol.* **6**, e105.
Carricaburu, V., Lamia, K. A., Lo, E., Favereaux, L., Payrastre, B., Cantley, L. C. and Rameh, L. E. (2003). The phosphatidylinositol (PI)-5-phosphate 4-kinase type II enzyme controls insulin signaling by regulating PI-3,4,5-trisphosphate degradation. *Proc. Natl. Acad. Sci. USA* **100**, 9867-9872.
Chanez, A.-L., Hehl, A. B., Engstler, M. and Schneider, A. (2006). Ablation of the single dynamin of T. brucei blocks mitochondrial fission and endocytosis and leads to a precise cytokinesis arrest. *J. Cell Sci.* **119**, 2968-2974.
Collins, B. M., McCoy, A. J., Kent, H. M., Evans, P. R. and Owen, D. J. (2002). Molecular architecture and functional model of the endocytic AP2 complex. *Cell* **109**, 523-535.
Cremona, O., Di Paolo, G., Wenk, M. R., Lüthi, A., Kim, W. T., Takei, K., Daniell, L., Nemoto, Y., Shears, S. B., Flavell, R. A. et al. (1999). Essential role of phosphoinositide metabolism in synaptic vesicle recycling. *Cell* **99**, 179-188.
De Camilli, P., Chen, H., Hyman, J., Panepucci, E., Bateman, A. and Brunger, A. T. (2002). The ENTH domain. *FEBS Lett.* **513**, 11-18.
Dell'Angelica, E. C., Klumperman, J., Stoorvogel, W. and Bonifacino, J. S. (1998). Association of the AP-3 adaptor complex with clathrin. *Science* **280**, 431-434.
Demmel, L., Melak, M., Kotisch, H., Fendos, J., Reipert, S. and Warren, G. (2011). Differential selection of Golgi proteins by COPII Sec24 isoforms in procyclic Trypanosoma brucei. *Traffic* **12**, 1575-1591.
Denk, W. and Horstmann, H. (2004). Serial block-face scanning electron microscopy to reconstruct three-dimensional tissue nanostructure. *PLoS Biol.* **2**, e329.
Di Paolo, G. and De Camilli, P. (2006). Phosphoinositides in cell regulation and membrane dynamics. *Nature* **443**, 651-657.
Doughman, R. L., Firestone, A. J. and Anderson, R. A. (2003). Phosphatidylinositol phosphate kinases put PI4,5P(2) in its place. *J. Membr. Biol.* **194**, 77-89.
Duszenko, M., Ivanov, I. E., Ferguson, M. A., Plesken, H. and Cross, G. A. (1988). Intracellular transport of a variant surface glycoprotein in Trypanosoma brucei. *J. Cell Biol.* **106**, 77-86.
Edeling, M. A., Mishra, S. K., Keyel, P. A., Steinhauser, A. L., Collins, B. M., Roth, R., Heuser, J. E., Owen, D. J. and Traub, L. M. (2006a). Molecular switches involving the AP-2 beta2 appendage regulate endocytic cargo selection and clathrin coat assembly. *Dev. Cell* **10**, 329-342.
Edeling, M. A., Smith, C. and Owen, D. (2006b). Life of a clathrin coat: insights from clathrin and AP structures. *Nat. Rev. Mol. Cell Biol.* **7**, 32-44.
Engstler, M., Thilo, L., Weise, F., Grünfelder, C. G., Schwarz, H., Boshart, M. and Overath, P. (2004). Kinetics of endocytosis and recycling of the GPI-anchored variant surface glycoprotein in Trypanosoma brucei. *J. Cell Sci.* **117**, 1105-1115.
Engstler, M., Pfohl, T., Herminghaus, S., Boshart, M., Wiegertjes, G., Heddergott, N. and Overath, P. (2007). Hydrodynamic flow-mediated protein sorting on the cell surface of trypanosomes. *Cell* **131**, 505-515.
Esson, H. J., Morriswood, B., Yavuz, S., Vidilaseris, K., Dong, G. and Warren, G. (2012). Morphology of the trypanosome bilobe, a novel cytoskeletal structure. *Eukaryot. Cell* **11**, 761-772.
Faulhammer, F., Kanjilal-Kolar, S., Knödler, A., Lo, J., Lee, Y., Konrad, G. and Mayinger, P. (2007). Growth control of Golgi phosphoinositides by reciprocal localization of sac1 lipid phosphatase and pik1 4-kinase. *Traffic* **8**, 1554-1567.
Ferguson, M. A., Duszenko, M., Lamont, G. S., Overath, P. and Cross, G. A. (1986). Biosynthesis of Trypanosoma brucei variant surface glycoproteins. N-glycosylation and addition of a phosphatidylinositol membrane anchor. *J. Biol. Chem.* **261**, 356-362.
Ford, M. G., Pearse, B. M., Higgins, M. K., Vallis, Y., Owen, D. J., Gibson, A., Hopkins, C. R., Evans, P. R. and McMahon, H. T. (2001). Simultaneous binding of PtdIns(4,5)P2 and clathrin by AP180 in the nucleation of clathrin lattices on membranes. *Science* **291**, 1051-1055.
Ford, M. G. J., Mills, I. G., Peter, B. J., Vallis, Y., Praefcke, G. J. K., Evans, P. R. and McMahon, H. T. (2002). Curvature of clathrin-coated pits driven by epsin. *Nature* **419**, 361-366.
Fruman, D. A., Meyers, R. E. and Cantley, L. C. (1998). Phosphoinositide kinases. *Annu. Rev. Biochem.* **67**, 481-507.
Futter, C. E., Connolly, C. N., Cutler, D. F. and Hopkins, C. R. (1995). Newly synthesized transferrin receptors can be detected in the endosome before they appear on the cell surface. *J. Biol. Chem.* **270**, 10999-11003.
Gabernet-Castello, C., Dacks, J. B. and Field, M. C. (2009). The single ENTH-domain protein of trypanosomes; endocytic functions and evolutionary relationship with epsin. *Traffic* **10**, 894-911.
Gaidarov, I. and Keen, J. H. (1999). Phosphoinositide-AP-2 interactions required for targeting to plasma membrane clathrin-coated pits. *J. Cell Biol.* **146**, 755-764.
García-Salcedo, J. A., Pérez-Morga, D., Gijón, P., Dilbeck, V., Pays, E. and Nolan, D. P. (2004). A differential role for actin during the life cycle of Trypanosoma brucei. *EMBO J.* **23**, 780-789.
Geuze, H. J., Slot, J. W., van der Ley, P. A. and Scheffer, R. C. (1981). Use of colloidal gold particles in double-labeling immunoelectron microscopy of ultrathin frozen tissue sections. *J. Cell Biol.* **89**, 653-665.
Griffiths, G. and Simons, K. (1986). The trans Golgi network: sorting at the exit site of the Golgi complex. *Science* **234**, 438-443.
Grünfelder, C. G., Engstler, M., Weise, F., Schwarz, H., Stierhof, Y.-D., Boshart, M. and Overath, P. (2002). Accumulation of a GPI-anchored protein at the cell surface requires sorting at multiple intracellular levels. *Traffic* **3**, 547-559.
Gull, K. (2003). Host-parasite interactions and trypanosome morphogenesis: a flagellar pocketful of goodies. *Curr. Opin. Microbiol.* **6**, 365-370.
Guo, W., Roth, D., Walch-Solimena, C. and Novick, P. (1999). The exocyst is an effector for Sec4p, targeting secretory vesicles to sites of exocytosis. *EMBO J.* **18**, 1071-1080.
He, C. Y., Pypaert, M. and Warren, G. (2005). Golgi duplication in Trypanosoma brucei requires Centrin2. *Science* **310**, 1196-1198.
Henley, G. L., Lee, C. M. and Takeuchi, A. (1978). Electron microscopy observations on Trypanosoma brucei: freeze-cleaving and thin-sectioning study of the apical part of the flagellar pocket. *Z. Parasitenkd.* **55**, 181-187.
Henne, W. M., Boucrot, E., Meinecke, M., Evergren, E., Vallis, Y., Mittal, R. and McMahon, H. T. (2010). FCHo proteins are nucleators of clathrin-mediated endocytosis. *Science* **328**, 1281-1284.
Hinshaw, J. E. and Schmid, S. L. (1995). Dynamin self-assembles into rings suggesting a mechanism for coated vesicle budding. *Nature* **374**, 190-192.
Hung, C.-H., Qiao, X., Lee, P.-T. and Lee, M. G.-S. (2004). Clathrin-dependent targeting of receptors to the flagellar pocket of procyclic-form Trypanosoma brucei. *Eukaryot. Cell* **3**, 1004-1014.
Ishihara, H., Shibasaki, Y., Kizuki, N., Katagiri, H., Yazaki, Y., Asano, T. and Oka, Y. (1996). Cloning of cDNAs encoding two isoforms of 68-kDa type I phosphatidylinositol-4-phosphate 5-kinase. *J. Biol. Chem.* **271**, 23611-23614.
Ishihara, H., Shibasaki, Y., Kizuki, N., Wada, T., Yazaki, Y., Asano, T. and Oka, Y. (1998). Type I phosphatidylinositol-4-phosphate 5-kinases. Cloning of the third isoform and deletion/substitution analysis of members of this novel lipid kinase family. *J. Biol. Chem.* **273**, 8741-8748.
Jackson, D. G., Owen, M. J. and Voorheis, H. P. (1985). A new method for the rapid purification of both the membrane-bound and released forms of the variant surface glycoprotein from Trypanosoma brucei. *Biochem. J.* **230**, 195-202.
Katoh, K., Kuma, K., Toh, H. and Miyata, T. (2005). MAFFT version 5: improvement in accuracy of multiple sequence alignment. *Nucleic Acids Res.* **33**, 511-518.
Kelly, B. T., McCoy, A. J., Späte, K., Miller, S. E., Evans, P. R., Höning, S. and Owen, D. J. (2008). A structural explanation for the binding of endocytic dileucine motifs by the AP2 complex. *Nature* **456**, 976-979.
Knuehl, C., Chen, C.-Y., Manalo, V., Hwang, P. K., Ota, N. and Brodsky, F. M. (2006). Novel binding sites on clathrin and adaptors regulate distinct aspects of coat assembly. *Traffic* **7**, 1688-1700.
Kohl, L., Sherwin, T. and Gull, K. (1999). Assembly of the paraflagellar rod and the flagellum attachment zone complex during the Trypanosoma brucei cell cycle. *J. Eukaryot. Microbiol.* **46**, 105-109.
Kosaka, T. and Ikeda, K. (1983). Reversible blockage of membrane retrieval and endocytosis in the garland cell of the temperature-sensitive mutant of Drosophila melanogaster, shibirets1. *J. Cell Biol.* **97**, 499-507.
Krauss, M., Kinuta, M., Wenk, M. R., De Camilli, P., Takei, K. and Haucke, V. (2003). ARF6 stimulates clathrin/AP-2 recruitment to synaptic membranes by activating phosphatidylinositol phosphate kinase type Igamma. *J. Cell Biol.* **162**, 113-124.
Krauss, M., Kukhtina, V., Pechstein, A. and Haucke, V. (2006). Stimulation of phosphatidylinositol kinase type I-mediated phosphatidylinositol (4,5)-bisphosphate synthesis by AP-2mu-cargo complexes. *Proc. Natl. Acad. Sci. USA* **103**, 11934-11939.
Kremer, J. R., Mastronarde, D. N. and McIntosh, J. R. (1996). Computer visualization of three-dimensional image data using IMOD. *J. Struct. Biol.* **116**, 71-76.
Kunz, J., Wilson, M. P., Kisseleva, M., Hurley, J. H., Majerus, P. W. and Anderson, R. A. (2000). The activation loop of phosphatidylinositol phosphate kinases determines signaling specificity. *Mol. Cell* **5**, 1-11.
Lacomble, S., Vaughan, S., Gadelha, C., Morphew, M. K., Shaw, M. K., McIntosh, J. R. and Gull, K. (2009). Three-dimensional cellular architecture of the flagellar pocket and associated cytoskeleton in trypanosomes revealed by electron microscope tomography. *J. Cell Sci.* **122**, 1081-1090.
Lacomble, S., Vaughan, S., Gadelha, C., Morphew, M. K., Shaw, M. K., McIntosh, J. R. and Gull, K. (2010). Basal body movements orchestrate membrane organelle division and cell morphogenesis in Trypanosoma brucei. *J. Cell Sci.* **123**, 2884-2891.
Lemmon, M. A., Ferguson, K. M., O'Brien, R., Sigler, P. B. and Schlessinger, J. (1995). Specific and high-affinity binding of inositol phosphates to an isolated pleckstrin homology domain. *Proc. Natl. Acad. Sci. USA* **92**, 10472-10476.
Levine, T. P. and Munro, S. (2002). Targeting of Golgi-specific pleckstrin homology domains involves both PtdIns 4-kinase-dependent and -independent components. *Curr. Biol.* **12**, 695-704.
Liou, W., Geuze, H. J. and Slot, J. W. (1996). Improving structural integrity of cryosections for immunogold labeling. *Histochem. Cell Biol.* **106**, 41-58.
Loijens, J. C. and Anderson, R. A. (1996). Type I phosphatidylinositol-4-phosphate 5-kinases are distinct members of this novel lipid kinase family. *J. Biol. Chem.* **271**, 32937-32943.

Marchetti, M. A., Tschudi, C., Kwon, H., Wolin, S. L. and Ullu, E. (2000). Import of proteins into the trypanosome nucleus and their distribution at karyokinesis. *J. Cell Sci.* **113**, 899-906.
Matthews, K. R. (2005). The developmental cell biology of Trypanosoma brucei. **118**, 283-290.
McLaughlin, S. and Murray, D. (2005). Plasma membrane phosphoinositide organization by protein electrostatics. *Nature* **438**, 605-611.
McMahon, H. T. and Boucrot, E. (2011). Molecular mechanism and physiological functions of clathrin-mediated endocytosis. *Nat. Rev. Mol. Cell Biol.* **12**, 517-533.
Milosevic, I., Giovedi, S., Lou, X., Raimondi, A., Collesi, C., Shen, H., Paradise, S., O'Toole, E., Ferguson, S., Cremona, O. et al. (2011). Recruitment of endophilin to clathrin-coated pit necks is required for efficient vesicle uncoating after fission. *Neuron* **72**, 587-601.
Morgan, G. W., Goulding, D. and Field, M. C. (2004). The single dynamin-like protein of Trypanosoma brucei regulates mitochondrial division and is not required for endocytosis. *J. Biol. Chem.* **279**, 10692-10701.
Morriswood, B., He, C. Y., Sealey-Cardona, M., Yelinek, J., Pypaert, M. and Warren, G. (2009). The bilobe structure of Trypanosoma brucei contains a MORN-repeat protein. *Mol. Biochem. Parasitol.* **167**, 95-103.
Morriswood, B., Havlicek, K., Demmel, L., Yavuz, S., Sealey-Cardona, M., Vidilaseris, K., Anrather, D., Kostan, J., Djinovic-Carugo, K., Roux, K. J. et al. (2013). Novel bilobe components in Trypanosoma brucei identified using proximity-dependent biotinylation. *Eukaryot. Cell* **12**, 356-367.
Mulkearns, E. E. and Cooper, J. A. (2012). FCH domain only-2 organizes clathrin-coated structures and interacts with Disabled-2 for low-density lipoprotein receptor endocytosis. *Mol. Biol. Cell* **23**, 1330-1342.
Nasuhoglu, C., Feng, S., Mao, J., Yamamoto, M., Yin, H. L., Earnest, S., Barylko, B., Albanesi, J. P. and Hilgemann, D. W. (2002). Nonradioactive analysis of phosphatidylinositides and other anionic phospholipids by anion-exchange high-performance liquid chromatography with suppressed conductivity detection. *Anal. Biochem.* **301**, 243-254.
Overath, P. and Engstler, M. (2004). Endocytosis, membrane recycling and sorting of GPI-anchored proteins: Trypanosoma brucei as a model system. *Mol. Microbiol.* **53**, 735-744.
Punta, M., Coggill, P. C., Eberhardt, R. Y., Mistry, J., Tate, J., Boursnell, C., Pang, N., Forslund, K., Ceric, G., Clements, J. et al. (2012). The Pfam protein families database. *Nucleic Acids Res.* **40**, D290-D301.
Redmond, S., Vadivelu, J. and Field, M. C. (2003). RNAit: an automated web-based tool for the selection of RNAi targets in Trypanosoma brucei. *Mol. Biochem. Parasitol.* **128**, 115-118.
Rosenthal, J. A., Chen, H., Slepnev, V. I., Pellegrini, L., Salcini, A. E., Di Fiore, P. P. and De Camilli, P. (1999). The epsins define a family of proteins that interact with components of the clathrin coat and contain a new protein module. *J. Biol. Chem.* **274**, 33959-33965.
Saint-Pol, A., Yélamos, B., Amessou, M., Mills, I. G., Dugast, M., Tenza, D., Schu, P., Antony, C., McMahon, H. T., Lamaze, C. et al. (2004). Clathrin adaptor epsinR is required for retrograde sorting on early endosomal membranes. *Dev. Cell* **6**, 525-538.
Schwarz, H., Giese, G., Müller, H., Koenen, M. and Witzemann, V. (2000). Different functions of fetal and adult AChR subtypes for the formation and maintenance of neuromuscular synapses revealed in epsilon-subunit-deficient mice. *Eur. J. Neurosci.* **12**, 3107-3116.
Seedorf, M., Damelin, M., Kahana, J., Taura, T. and Silver, P. A. (1999). Interactions between a nuclear transporter and a subset of nuclear pore complex proteins depend on Ran GTPase. *Mol. Cell. Biol.* **19**, 1547-1557.
Stauffer, T. P., Ahn, S. and Meyer, T. (1998). Receptor-induced transient reduction in plasma membrane PtdIns(4,5)P2 concentration monitored in living cells. *Curr. Biol.* **8**, 343-346.
Stefan, C. J., Manford, A. G., Baird, D., Yamada-Hanff, J., Mao, Y. and Emr, S. D. (2011). Osh proteins regulate phosphoinositide metabolism at ER-plasma membrane contact sites. *Cell* **144**, 389-401.
Steverding, D. (2000). The transferrin receptor of Trypanosoma brucei. *Parasitol. Int.* **48**, 191-198.
Stimpson, H. E. M., Toret, C. P., Cheng, A. T., Pauly, B. S. and Drubin, D. G. (2009). Early-arriving Syp1p and Ede1p function in endocytic site placement and formation in budding yeast. *Mol. Biol. Cell* **20**, 4640-4651.
Sweitzer, S. M. and Hinshaw, J. E. (1998). Dynamin undergoes a GTP-dependent conformational change causing vesiculation. *Cell* **93**, 1021-1029.
Taguchi, T. (2013). Emerging roles of recycling endosomes. *J. Biochem.* **153**, 505-510.
TerBush, D. R., Maurice, T., Roth, D. and Novick, P. (1996). The Exocyst is a multiprotein complex required for exocytosis in Saccharomyces cerevisiae. *EMBO J.* **15**, 6483-6494.
ter Haar, E., Harrison, S. C. and Kirchhausen, T. (2000). Peptide-in-groove interactions link target proteins to the beta-propeller of clathrin. *Proc. Natl. Acad. Sci. USA* **97**, 1096-1100.
Thieman, J. R., Mishra, S. K., Ling, K., Doray, B., Anderson, R. A. and Traub, L. M. (2009). Clathrin regulates the association of PIPKIgamma661 with the AP-2 adaptor beta2 appendage. *J. Biol. Chem.* **284**, 13924-13939.
Várnai, P. and Balla, T. (1998). Visualization of phosphoinositides that bind pleckstrin homology domains: calcium- and agonist-induced dynamic changes and relationship to myo-[3H]inositol-labeled phosphoinositide pools. *J. Cell Biol.* **143**, 501-510.
Wang, S. and Hsu, S. C. (2006). The molecular mechanisms of the mammalian exocyst complex in exocytosis. *Biochem. Soc. Trans.* **34**, 687-690.
Wang, Z., Morris, J. C., Drew, M. E. and Englund, P. T. (2000). Inhibition of Trypanosoma brucei gene expression by RNA interference using an integratable vector with opposing T7 promoters. *J. Biol. Chem.* **275**, 40174-40179.
Wasiak, S., Legendre-Guillemin, V., Puertollano, R., Blondeau, F., Girard, M., de Heuvel, E., Boismenu, D., Bell, A. W., Bonifacino, J. S. and McPherson, P. S. (2002). Enthoprotin: a novel clathrin-associated protein identified through subcellular proteomics. *J. Cell Biol.* **158**, 855-862.
Wenk, M. R., Pellegrini, L., Klenchin, V. A., Di Paolo, G., Chang, S., Daniell, L., Arioka, M., Martin, T. F. and De Camilli, P. (2001). PIP kinase Igamma is the major PI(4,5)P(2) synthesizing enzyme at the synapse. *Neuron* **32**, 79-88.
Wirtz, E., Leal, S., Ochatt, C. and Cross, G. A. (1999). A tightly regulated inducible expression system for conditional gene knock-outs and dominant-negative genetics in Trypanosoma brucei. *Mol. Biochem. Parasitol.* **99**, 89-101.
Zankel, A., Kraus, B., Poelt, P., Schaffer, M. and Ingolic, E. (2009). Ultramicrotomy in the ESEM, a versatile method for materials and life sciences. *J. Microsc.* **233**, 140-148.
Zoncu, R., Perera, R. M., Sebastian, R., Nakatsu, F., Chen, H., Balla, T., Ayala, G., Toomre, D. and De Camilli, P. V. (2007). Loss of endocytic clathrin-coated pits upon acute depletion of phosphatidylinositol 4,5-bisphosphate. *Proc. Natl. Acad. Sci. USA* **104**, 3793-3798.